Spectral Reflectance of Soil

Jerzy Cierniewski

1 Introduction

The reflectance spectra of soils in the visible and near infrared (VNIR) and shortwave infrared (SWIR) contain information on mineral groups, organic matter and soil texture. The spectra collected by airborne hyperspectral scanners were corrected for the influence of the atmosphere and the non-Lambertian behavior of soil surfaces whose real roughness formed is by agricultural tools; this made it possible to determine the content of soil organic carbon, calcium carbonate and textural clay with an accuracy expressed by a coefficient of determination (R^2) of 60–75% (Schwanghart and Jarmer 2011; Gomez et al. 2008a, b; Selige et al. 2006). The same soils' spectra obtained in the laboratory on air-dried, smooth soil samples using a spectroradiometer with a contact-probe sensor show a higher overall reflectance (mainly due to the effect of their roughness having been minimized) and this allowed the contents of the above mentioned components to be determined with an R^2 of about 10–20% higher. Quantitative soil properties in both of the above situations were obtained by multivariate linear regression analysis of the reflectance spectra with respect to such chemical and physical data, using, for example, partial-square regression, spline signal regression and support vector machine (Selige et al. 2006; Stevens et al. 2010). As part of a research project aimed at quantifying the annual dynamics of shortwave radiation reflected from arable lands on a global scale taking into account their roughness, the soil spectra obtained in the laboratory were also used to predict the variation of the diurnal broadband blue-sky albedo of soils (α) in clear-sky conditions. This variation allows for more precise calculation of the average diurnal α values of soils and, on this basis, also of their average α values over longer periods of several days, a month, a season or a year. It can be useful for modeling the climate on a global

J. Cierniewski (✉)
Department of Soil Science and Remote Sensing of Soils, Adam Mickiewicz University, Bogumiła Krygowskiego 10, 61-680 Poznań, Poland
e-mail: ciernje@amu.edu.pl

A. Kokhanovsky (ed.), *Springer Series in Light Scattering*,
Springer Series in Light Scattering,
https://doi.org/10.1007/978-3-030-38696-2_4

scale, which in light of the statement of Sellers et al. (1995) require α values with an accuracy of better than $\pm 2\%$. The laboratory reflectance spectra of geo-referenced topsoil samples, which are stored together with the chemical and physical attributes of these samples in soil spectral libraries (SSL) on national and continental scales, were used in this project. The example of this project shows that information coded in the soil spectra collected in the Global SSL not only "can be associated to land cover and its global geographic distribution, which may acting as a surrogate for global climate variability" (Viscarra Rossel et al. 2016), but can also be directly used for quantification dynamics of shortwave radiation reflected from one of the Earth's land surface components—bare arable lands. Although bare arable soils occur in relatively short periods on these conventionally cultivated lands (Cierniewski et al. 2018c; Cierniewski and Ceglarek 2018), due to their large total surface they can significantly affect the energy transfer between them and the atmosphere (expressed by their α), depending on their spectral reflectance properties, including their roughness formed by agricultural tools. Smoothing rough arable lands that have previously been deeply plowed with, for example, a smoothing harrow increases their α, resulting in a lower amount of shortwave radiation being absorbed by their surface layer. Those surfaces emit less long-wave radiation, leading to a reduction in their temperature, which can modify the Earth's climate (Desjardins 2009; Farmer and Cook 2013).

2 Reflectance Spectra

The proportions between amounts of radiant flux of electromagnetic radiation in specific wavelength (λ) incident on an object that are reflected from its surface (ρ_λ), absorbed by the surface and transmitted by the surface vary relative to the wavelength in a way that is particular to each of Earth object (Lillesand et al. 2004). The reflectance has a directional character and as such depends on the direction of surface illumination and of its observation by a sensor. The reflectance spectrum of an object in the optical domain (0.35–2.5 μm) is the collection of the $\rho_{\Omega,\lambda}$ values describing the ratio of the reflected radiant flux from its surface (L) into solid angle (Ω) to the radiant flux incident on its surface (E) into Ω for a specific λ (Palmer 1982):

$$\rho_{\Omega,\lambda} = \frac{L_{\Omega,\lambda}}{E_{\Omega,\lambda}} \tag{1}$$

Each object has a specific spectrum, which can distinguish the object from others, identify it and determine its properties. The higher the number of spectral bands and the narrower the ranges that are taken into account, the more accurate this identification will be. The significant technological advances that have occurred over the past 30 years in the construction of spectrometers and radiometers working in visible and near infrared (VNIR: 0.35–1.1 μm) and shortwave infrared (SWIR: 1.1–2.5 μm),

enabled the development of remote sensing methods for identification of Earth's objects and their properties using the spectra measured by these instruments.

2.1 Factors Affecting Soil Reflectance Spectra

Soil is the medium for plant growth, and a habitat for many insects and other organisms. It provides us food, fuel and fibers. It acts as a system for carbon storage and filtration of surface water and regulates the emissions of greenhouse gases, and thus affects the Earth's climate. Soil degradation and increasing urbanization disturb the agro-ecological balance (Viscarra Rossel et al. 2016). In order to manage soils in a sustainable manner (UN Sustainable Development Knowledge 2015) and thus preserve them for future generations, it is important to have a deeper understanding of the processes and function they perform. As a natural body of Earth material, soil consists of minerals and organic substances. These constituents have an influence on the soil's spectral reflectance pattern. Nearly all optical shortwave radiation incident on soil surfaces is either absorbed or reflected, and only a little part is transmitted. Strong absorption of the radiation is mainly caused by the solid phase of soils consisting of opaque mineral particles covered with soil organic matter (SOM) in its various stages of decomposition, as well as the soil liquid phase that consists of water and dissolved ions in various amounts. Soil pores not filled with the liquid phase are filled with soil air, constituting the gas phase, i.e. soil air of similar composition to that of atmospheric air but with varying concentrations of oxygen and carbon dioxide depending on the biochemical activity at the root zone. The pores filled with soil air can act as specific optical fibers, having their origin on soil surfaces and ending at a depth of 1–10 mm (Mikhajlova and Orlov 1986). Shortwave radiation is mostly absorbed in such a thin layer of soils, usually in the horizon of SOM accumulation.

The shape and overall level of soil spectra in the solar reflective radiation range is the result of the physical process of light scattering in the VNIR region, depending on the size of soil particles, and their shape and distribution in soil materials (Ben-Dor et al. 1999). Soil components such as iron oxides or organic matter determine the slope of the spectra at the wide wavelength range lower than 1.0 μm. The chemical processes associated with the absorption of light by soil components are revealed in the narrow ranges of the SWIR region of soil spectra. The presence of water molecules contained in the soil in the form of hygroscopic water is clearly visible around 1.4 and 1.9 m, and for example, clay minerals and calcite around 2.2 and 2.3 m (Ben-Dor 2002).

2.1.1 Soil Organic Matter

The spectral reflectance level of soils in the VNIR region decreases as their SOM content increases. If the SOM content is lower than 2%, a small increase results in a strong decrease in the reflectance of such soils (Al-Abbas et al. 1972; Fedchenko

1982). More and more fragments of usually bright mineral particles in such soils are covered by dark SOM; hence the reflectance of these soils is less and less similar to that of their parent material. A growth in the amount of SOM from 2 to 4% results in a further increase in the surrounding of the parent material particles by SOM. If the last of these particles are completely surrounded by SOM, and this occurs at an SOM content of about 5–6%, a further increase in its content very slightly decreases the reflectance of soils. The minimum of this reflectance is observed for soils with SOM content of about 10–12% (Swain 1978; Latz et al. 1984). Vinogradov (1981), Orlov and Sukhanova (1983) and Baumgardner et al. (1986) described the relation between the SOM of soils and their reflectance in the VNIR using an exponential function. The reflectance level of bare soils also depends on the quality of SOM, resulting from the proportion of the two main fractions of humus compounds, humic and fulvic acids (Obukhov and Orlov 1964; Białousz and Girard 1978; Bauer et al. 1981; Vinogradov 1981; Mikhajlova and Orlov 1986). Humic acids absorb more visible radiation than do fulvic acids: the latter reflect from 1.5 to 2 times more radiation in the range of blue waves and from 3 to 4 times more in the range of green and red waves (Obukhov and Orlov 1964). The differentiation in the reflectance of these fractions of humus compounds is explained by the difference in their molecular structure. Molecules of humic acids have a spatially more complicated structure than fulvic acids, so that they are optically denser and thus absorb more shortwave radiation (Kononova 1956, 1963). The higher the proportion of humic acid to fulvic acid in SOM (expressing the SOM quality) and the higher the SOM content, the lower the spectral reflectance of bare soils. The relations between the spectral reflectance of soils and their SOM content were determined on the basis of soil samples of various SOM qualities. Thus, the wavelength ranges for which these relations were closest were found in different wavelength ranges. Al-Abbas et al. (1972), Vinogradov (1981), Mikhajlova and Orlov (1986) defined this range for orange and red waves (between 0.6 and 0.75 μm), while Henderson et al. (1992) defined it for the wider range from blue to red wavelength (0.43–0.69 μm). Close relations between SOM and soil reflectance level was also found in the SWIR region. Dalal and Henry (1986) determined it between 1.7 and 2.05 μm, and Morra et al. (1991) between 1.73 and 2.43 μm.

Another course of the relationship between the spectral reflectance level of soils and their SOM content has been observed in peat soils with different levels of organic matter decomposition. With the progress of decomposition of peat materials from fibric through hemic to sapric, a pronounced decrease in the spectral reflectance of such materials was observed (Baumgardner et al. 1986). Mikhajlova and Orlov (1986) reported a minimum of this reflectance for peat material with an SOM content of 60–80%, which corresponds to sapric material.

2.1.2 Iron Oxides

Among the iron compounds, iron oxides in the form of non-aluminosilicate minerals such as goethite and hematite, as well as poorly crystallized and amorphous forms that surround the mineral soil particles, have the strongest effects on spectral reflectance

of soils in VNIR (Karmanova 1981; Mikhajlova and Orlov 1986). The content of iron oxides in soils reduces their spectral reflectance mainly in the yellow and red waves range from 0.52 to 0.62 μm (Obukhov and Orlov 1964; Krishna Murti and Satyanarayana 1971; White 1971). However, this reduction has a selective character (Cipra et al. 1971). It is observed in the yellow waves for strongly hydrated oxides, among which goethite dominates, and in the red waves for less hydrated oxides, where hematite has the largest share. Other absorption bands occur around 0.7 and 0.87 μm (Stoner et al. 1980), and there is additional absorption in the middle infrared wavelengths (Hunt and Salisbury 1970; Mulders 1987).

2.1.3 Calcium Carbonates

Clark et al. (2003) found that calcium carbonate ($CaCO_3$) most strongly absorbs shortwave radiation at wavelengths of 2.21 and 2.35 μm (2008). $CaCO_3$ differently affects the spectral reflectance of soils in laboratory conditions than in field conditions. In the laboratory, the higher the $CaCO_3$ content in the soil samples with disturbed aggregates, the higher their reflectance (Lagacherie et al. 2008). Cierniewski and Kuśnierek (2010) reported that this relationship in laboratory conditions is almost directly proportional in the spectral region above 1 μm. Bialousz (1978) found that the relation in field conditions becomes directly proportional if the $CaCO_3$ content is higher than 20%. If the content is lower than this value, this relation is inversely proportional and indirect. This author explained that $CaCO_3$ is conducive to the formation of soil aggregates. These aggregates increase the surface roughness of the soil, thus reducing of soil reflectance despite the high spectral reflectance of this substance. $CaCO_3$ promotes the formation and accumulation of permanent connections between humus compounds, iron oxides and clay fraction.

2.1.4 Moisture of Soil Surface

Generally, a decrease in the moisture of the soil surface causes an increase in the overall level of their reflectance spectra (Idso et al. 1975; Baumgardner et al. 1986; Music and Pelletier 1986). The darkening of a moist soil in VNIR, where water absorption is minimal, is mainly due to the increased probability of the light scattering forward, deeper into the depth, which increases multiply scattering, increases the probability of absorption and decreases the reflectance of the soil (Twomey et al. 1986; Lekner and Dorf 1988; Philpot 2010). The tendency for increased scattering of such soil is further increased by the presence of air–water boundaries in the soil pore spaces. If the soil water content (SWC) decreases from the state of full saturation (FS) to the state of field capacity (FC), the level of soil spectral reflectance does not change (Tolchelnikov 1974; Vinogradov 1983) or decreases slightly (Cierniewski 1988, 1993). The increase in the level of the soil spectra is most pronounced if SWC decreases from FC to the state of maximum hygroscopicity (MH) (Bowers and Smith 1972; Tolchelnikov 1974). If SWC continues to decline to the absolutely

dry state (AD), the reflectance level increases slightly (Vinogradov 1976, 1983) or is unnoticeable (Tolchelnikov 1974; Cierniewski 1985, 1988; Cierniewski et al. 1988). The aforementioned soil moisture states, depending on their texture, correspond to different SMC values expressed as the proportion mass of water to mass of dry soil. For example, sand and clay get MH at SMC of about 1%, and 6%, respectively (Vinogradov 1983). However, the same materials obtain FC at SMC of around 5 and 22%. Such different courses of dependence between the spectral reflectance level of soils and their moisture in these three SWC ranges are explained by the dissimilarity between the water forms that occur there. In the SWC range from FS to FC there is gravitational water. In the range from FC to MH there is capillary water in fine pores, and in the range from MH to AD there is only chemically combined water, water in the form of vapor and hygroscopic water.

Moisture of the soil surface is the most dynamically changing factor determining the overall level of reflectance spectra of soils in field conditions (Milfred and Kiefer 2010). It is observed especially in the summer when the surface layer of soils quickly achieves a state of air-dried soil (Andronikov 1979). The increase in soil spectral reflectance is more noticeable for light-colored soils with a lower SOM content than for dark-colored soils with a higher such content (Białousz and Girard 1978; Evans 1979; Mikhajlova and Orlov 1986).

2.1.5 Soil Surface Roughness

Soil Surface Roughness in the Laboratory

The property of soils that is unchanged over time is the particle size of their mineral fraction. Investigation of the effect of this size on the level of spectral reflectance in the laboratory on samples with natural structure having been destroyed shows clearly that their reflectance decreases with the increase in the diameter of soil particles. Bowers and Hanks (1965) analyzed fractionated soil material with particle diameters from 0.02 mm to 2.65 mm and determined that this relationship could be described using the exponential function, which represents the sharpest decline in the reflectance in the range of the diameters from 0.02 mm to 0.4 mm. This regularity was also confirmed by studies conducted by Piech and Walker (1974), who analyzed it in the VNIR range on seven loamy soil fractions separated on sieves with mesh diameters from 0.62 to 2 mm. Gerbermann and Weber (1979), investigated the spectral reflectance of soil samples prepared as mixtures from the clay and sandy fractions, and found that it is directly proportional to the content of their sandy fraction.

Soil samples with destroyed aggregates sieved through a 2-mm sieve are prepared to measure soil reflectance spectra in laboratory conditions in order to determine the soil texture and the content of such soil components as soil organic carbon (SOC), iron oxides and calcium carbonates (Ben-Dor et al. 2015). In order to minimize the impact of surface irregularities in these samples, receptors recording diffusion reflectance are most commonly used, such as for example a High-Brite Muglight receptor. Quantitative data on the properties of the investigated soils are extracted

from their reflectance spectra using multivariate linear regression analysis of the spectra against the chemical and physical data through several methods, such as for example partial squares regression (PLSR), spline signal regressions (PSR) and support vector machine (SVM) (Selige et al. 2006; Stevens et al. 2013). The proportion of sand and clay and the content of $CaCO_3$ and SOC can be determined in this way with the correctness expressed by coefficient of determination (R^2) reaching 0.85–0.95 (Selige et al. 2006; Gomez et al. 2008a, b; Schwanghart and Jarmer 2011). The correctness of these components in field conditions with a much greater natural roughness using airborne hyperspectral scanners shows a lower correctness of about 20% due to the influence of the atmosphere and the position of the sun and the direction of observation of studied soil surfaces.

Soil Surface Roughness in the Field

The influence of soil particle size on the spectral reflectance level of soils is usually almost imperceptible compared to the considerably stronger impact of their surface roughness caused by the existence of soil aggregates, clods and stones of various sizes under field conditions. In general, in these conditions, coarse texture (sandy) soils form smaller aggregates than those developed from fine texture (for example loamy), which form larger aggregates and clods. Smaller soil aggregates have a more compact, spherical shape than larger ones that have an irregular shape and are often cracked. As a result, the surfaces of these first soils appear smoother, with a higher spectral reflectance than especially those with a high density of large clods, which causes a clearly lower soil reflectance (Orlov 1969; Orlov et al. 1976). Thus, the particle size in the field indirectly and inversely affects the level of soil reflectance in contrast to its effect in the laboratory. Al-Abbas et al. (1972) noticed that a higher proportion of the sandy fraction significantly reduces the roughness of the soil surfaces, which increases their spectral reflectance. The reflectance from the soil surfaces with aggregates with a diameter from 2 to 10 mm is almost invariable, while with smaller aggregates it shows a clear differentiation (Orlov 1969; Curran et al. 1990). Generally, as the size of soil aggregates decreases, there is a clear increase in its spectral reflectance (Bowers and Hanks 1965; Piech and Walker 1974). The decrease in spectral reflectance of soils as a result of their roughness increasing is explained by the phenomenon of multiple reflections of the radiation that illuminates them. Most of the direct sunlight falling on the soil surfaces is absorbed by them and reflected from them, scattering it in all directions. This scattered radiation falling on them again is absorbed once again and reflected from them in a much smaller proportion than the original incident (Linden 1979; Cruse et al. 1980). The deep spaces between the large aggregates and clods are mostly "traps" for the sunlight directly falling on them (Orlov 1966; Coulson and Reynolds 1971).

Girard and Białousz (1989) presented the results of field studies showing how the effect of SOM content and soil surface moisture on the spectral reflectance of soils as their roughness changed. Epiphanio and Vitorello (1984) state that the correct

separation of dried soil surfaces from wet ones using remote sensing depends largely on their roughness.

Measurements of Soil Surface Roughness

In some climatic zones, the rain strongly changes the physical properties of the soil surface, reducing the infiltration of rainwater and increases the effects of water erosion through increased surface runoff (Collinet and Valentin 1985; Morgan 1985; Ghishi and Morgan 1986; Römkens and Wang 1986; Zobeck and Onstad 1987; Moreno et al. 2008; Thomsen et al. 2015). To effectively counteract these processes, the interdependencies between the state of roughness of selected soil surfaces and the possibilities of absorbing and storing water in their surface levels were investigated (Mitchell and Jones 1978; Onstad 1984). Decades ago, the variation of soil surface shape was measured along a direction using a profile meter with needles or a chain set (King 1979; Boiffin and Monnier 1986; Gilley and Kottwitz 1995). Desmet et al. (1988) suggested recording irregularities in soil surfaces using a paint sprayer on a vertically positioned piece of paper. Huang et al. (1988) and Bertuzzi et al. (1990) propose replacing or supplementing these simple tools with laser scanners constructed by them to measure the height of soil aggregates and clods in two-dimensional space along a single line with resolution of approximately 1 mm. Cierniewski et al. (2004), investigating the bidirectional reflectance of stony, sandy and silty surfaces in the Negev desert, measured their irregularities in three-dimensional space in a 1×1 cm grid with resolution of 1.5 mm using a laser device constructed at Ben Gurion University of the Negev. Some years later, Cierniewski et al. (2013) used a laser scanner camera, which measured the shape of desert and cultivated soil surfaces also in three-dimensional space with horizontal and vertical spatial resolutions of 1 mm. Currently, roughness of a soil surface is often examined by close-range digital photogrammetry using its images in three-dimensional space taken from over a dozen directions by a hand-held digital camera moving around the surface (Rieke-Zapp and Nearing 2005; Peter Heng et al. 2010; Gilliot et al. 2017). This photogrammetric method makes it possible to register soil surface irregularities with a similar spatial resolution of approximately 1 mm. Data obtained in this way allow digital elevation models (DEM) of the examined surfaces to be created, and these then become the basis for calculating soil surface roughness indices.

Soil Roughness Indices

The roughness of soil surfaces was described using quantitative indices. The standard deviation of the surface height (*HSD*) is the most common index for describing the soil surface roughness (Ulaby et al. 1982). The turtle index, representing the ratio of the actual length of the soil surface profile to the projected horizontal length of this profile, was proposed by Boiffin (1986). Later, Taconet and Ciarletti (2007) modified this index to describe the irregularities of a surface in two-dimensional space (T_{3D}),

defining it as the ratio of the real surface area within its basic DEM unit to its flat horizontal area. Other indices used to describe changes in soil surfaces roughness due to rainfall or sprinkler irrigation (caused by the breakdown of soil aggregates and the formation of soil crust) use a semivariogram analysis (Rosa et al. 2012; Croft et al. 2013; Vermang et al. 2013).

2.2 Bidirectional Reflectance Quantities

It is not only differences in the scale of soil surface irregularities between those measured under field conditions (with naturally formed aggregates and clods) and samples of the same soils measured in the laboratory (where the influence of their roughness is minimized by the destruction of soil aggregates) that cause distinctly different values of their bidirectional reflectance. Surfaces in the field are illuminated by direct sunbeams and diffuse light from the sky, while the samples in the laboratory are usually illuminated by a single collimated light source. The latter case can be described using the bidirectional reflectance distribution function (BRDF) that expressed the scattering of parallel (collimated) beams incident on a surface from one direction in the hemisphere into another direction in the hemisphere (Schaepman-Strub et al. 2006):

$$\mathrm{BRDF} = f_r(\Omega_i, \Omega_r) = f_r(\theta_i, \phi_i; \theta_r, \phi_r) = \frac{dL_r(\theta_i, \phi_i; \theta_r, \phi_r)}{dE_i(\theta_i, \phi_i)} \left[\mathrm{sr}^{-1}\right] \qquad (2)$$

However, it should be remembered that, in proposing BRDF as the fundamental quantity characterizing the reflecting properties of a surface, Nicodemus et al. (1977) formulated that the surface must be horizontally homogeneous, and that a uniform irradiance flux coming from a single direction covers a large enough area that radiation leaving the surface does not vary with horizontal position. Therefore, BRDF defines only the point of such a surface (Di Girolamo 2003) (Fig. 1). The two radiation environments are defined by two angles, depending on the direction of incidence of radiation of the light source Ω_i and the direction of reflected radiance coming to the sensor Ω_r. One of them refers to the zenith and symbolizes the light source zenith angle as θ_i and the view zenith angle as θ_r. The second is horizontal, and is called the azimuth angle, and indicates the light source azimuth angle as ϕ_i and the view azimuth angle as ϕ_r. By measuring the reflectance (ρ) of a sample surface such as, for example, soil, illuminating it with parallel beams from a single light source (as is usual in laboratory measurements), the bidirectional reflectance factor (BRF) is used. This unitless quantity is defined as the ratio of the reflected radiant flux (Φ_r) from the surface area dA to the radiant flux (Φ_r^{id}) reflected from an ideal lossless and diffuse (Lambertian) standard panel, illuminated and observed at the same directions as the sample surface being tested (Schaepman-Strub et al. 2006):

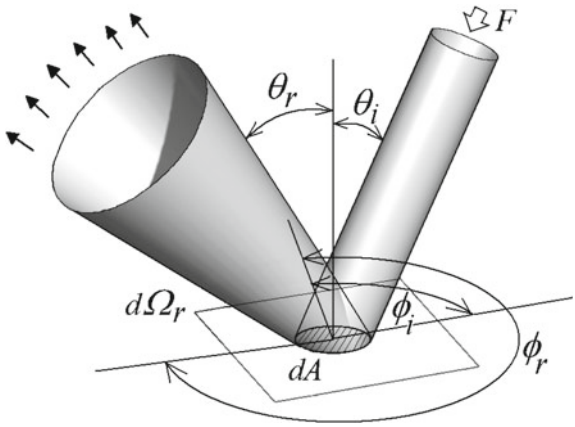

Fig. 1 Geometric relations between radiation of a collimated beam of flux density F incident at the zenith angle θ_i and the azimuth angle ϕ_i on an area dA, which is then scattered into solid angle dΩ_r in the direction, described by the zenith θ_r and azimuth ϕ_r angles

$$\mathrm{BRF} = \rho(\theta_i, \phi_i; \theta_r, \phi_r) = \frac{d\Phi_r(\theta_i, \phi_i; \theta_r, \phi_r)}{d\Phi_r^{id}(\theta_i, \phi_i)}. \tag{3}$$

Because there is no angular dependence on the ideal Lambertian surface (Palmer 1982; Jackson et al. 1987), the θ_r, ϕ_r angles for Φ_r^{id} were omitted. For surfaces illuminated by irradiation from the entire hemisphere, as in field conditions, Schaepman-Strub et al. (2006) suggest the use of hemispherical reflectance (HDRF):

$$\mathrm{HDRF} = \rho(\theta_i, \phi_i; 2\pi; \theta_r, \phi_r) = \frac{d\Phi_r(\theta_i, \phi_i; 2\pi; \theta_r, \phi_r)}{d\Phi_r^{id}(\theta_i, \phi_i; 2\pi)} \tag{4}$$

to describe the reflectance of such a surface. This quantity is similarly defined as the BRF, but it takes into account both the direct and the diffuse irradiance.

2.3 Non-lambertian Behavior of Soil Surfaces

Bare soil surfaces, like many natural and man-made objects, reveal their non-Lambertian behavior. Such surfaces show variation in their radiance due to the direction of their irradiation and the direction along which the reflected radiation is viewed by ground, air-borne and satellite sensors. Irregularities in soil surfaces caused by soil mineral particles, and especially by large aggregates and clods formed with the high participation of SOM, produce shadow areas where the solar beams do not directly reach the surface (Graetz and Gentle 1982; Norman et al. 1985; Otterman 1985; Cooper and Smith 1985; Jon Ranson et al. 1985; Cierniewski 1987, 1989; Milton and Webb 1987; Huete 1987; Pinty et al. 1989; Deering et al. 1989, 1990; Jackson et al. 1990; Irons et al. 1992) The spaces between the smaller aggregates are usually less intensely shaded than those between larger aggregates. Radiation leaving the shaded areas is many orders of magnitude smaller than radiation reflected

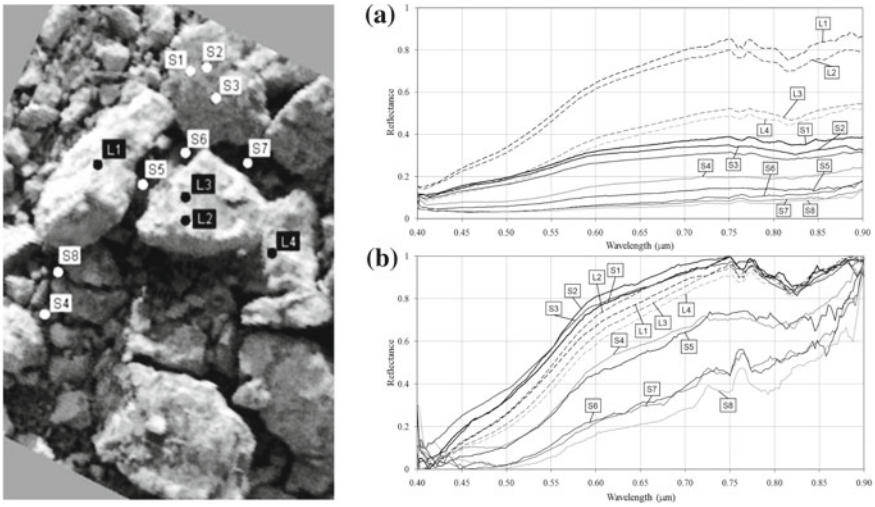

Fig. 2 Reflectance spectra of a soil surface at its sunlit [L] and shaded [S] fragments (**a**) and the same spectra normalized by the min–max method (**b**)

from sunlit soil fragments. A hyperspectral camera suspended over the ploughed soil observed this phenomenon (Cierniewski et al. 2010). Spectra related to the shaded soil fragments (marked 'S') show lower reflectance than the sunlit fragments (marked 'L'). The shape of these two categories of these spectra became similar to each other, if they were normalized by the min–max method (Fig. 2). Bare arable lands with dominant diffuse features usually appear brightest from the direction that gives the lowest proportion of shaded fragments. Those soil surfaces show a strong backscattering character with a reflectance peak towards the Sun position (the 'hot spot' direction) and decreasing reflectance in the direction away from the peak (Brennan and Bandeen 1970; Kriebel 1976; Milton and Webb 1987; Foody 1988). The non-Lambertian behavior of two soils, one uncultivated and smooth and another cultivated and moderate rough, is presented in Fig. 3 Irregularities in both their surfaces are spread non-directionally. Their reflectance distributions normalized to the nadir viewing in all possible directions for the chosen wavelength of 0.85 μm under clear-sky conditions at various solar zenith (θ_s) and azimuth (ϕ_s) angles were predicted by a hemispherical-directional reflectance model (Cierniewski et al. 2004). The larger the soil surface irregularities and the higher the θ_s, the higher the variation of the soil directional reflectance. The variation is greatest along the solar principal plane. Croft et al. (2012) presented a similar non-Lambertian behavior of soils in relation to almost the same roughness ranges as in the above examples, but their samples were subjected to artificial rainfall in laboratory conditions. Wang et al. (2012) showed examples of soil surface anisotropy analyzed in the laboratory on samples with undamaged surface structure as in field conditions in a much wider range of roughness. The result of a laboratory measurement experiment simulating

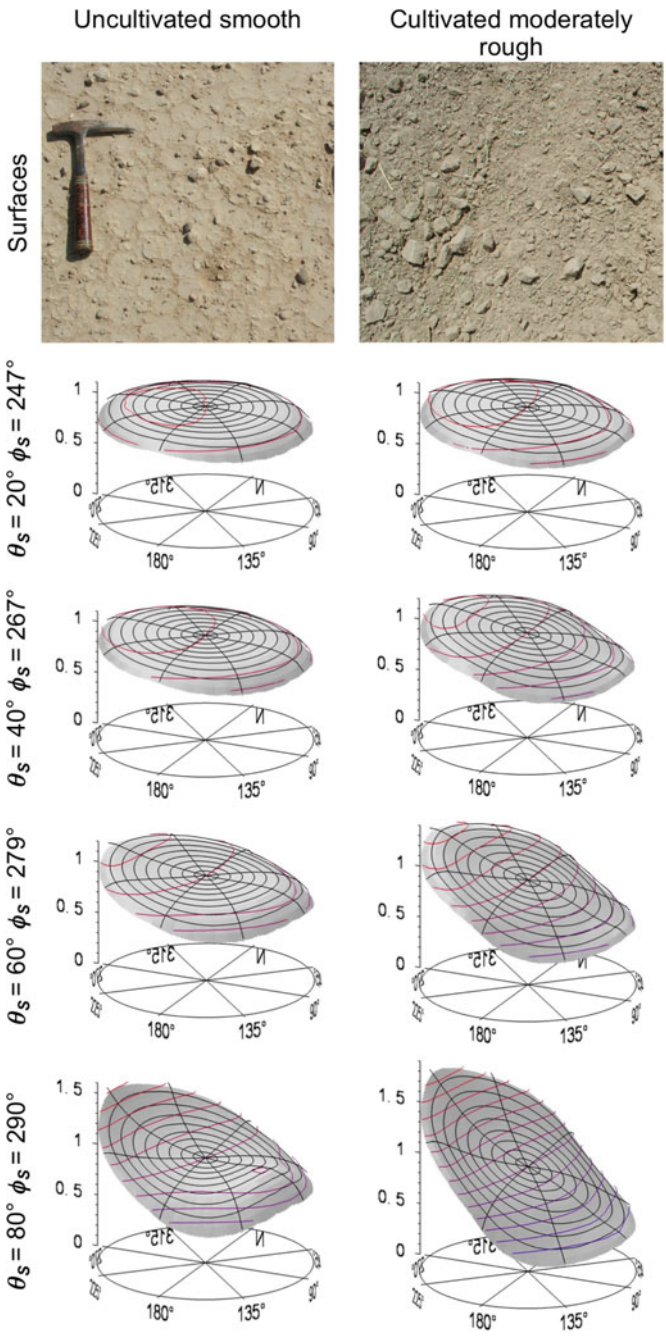

Fig. 3 Normalized directional reflectance distributions of soils for chosen wavelength of 0.85 μm under clear sky conditions at various solar zenith (θ_s) and azimuth (ϕ_s) angle predicted by a hemispherical-directional reflectance model (Cierniewski et al. 2004)

the behavior of the spectral reflectance of sandy soils with furrows treated by a harrow or a seeder show that a directional microrelief of those surfaces can additionally complicate the reflectance of those soils (Cierniewski and Guliński 2009). The level of the spectrum of such surfaces viewed at the nadir and illuminated by sunbeams coming along the furrows can be about 5–10% higher than for the same surface illuminated by sunbeams perpendicular to the furrows.

Spectral reflectance of desert soil surfaces can have both a backscattering and forward scattering character (Deering et al. 1990). The surfaces show maximum reflectance in the extreme forward scatter direction near the horizon if they are relatively smooth with strong specular features. Shoshany (1993) reported that different types of stony pavements and rocky surfaces investigated in various lighting conditions revealed an anisotropic reflection with a clear backscattering component.

Soil surface roughness is a particularly dynamically changing factor within arable land formed by agricultural tools. They create a specific micro-relief configuration, sometimes with a clear directional distribution of furrows. Cierniewski (2001) analyzed spectral reflectance of soils developed from loamy materials formed by a plow and different harrows (spike-tooth, rotary and disc). Matthias et al. (2000) found that the albedo of dried soil surfaces developed from fine sandy loam treated by a plow, a disk and a seedbed decreased its albedo by about 27%, 18% and 8%, respectively, in relation to the albedo of its smoothed surface. Surfaces of soils with a low cation-exchange capacity have an unstable structure, contributing easily to their roughness being reduced by rain or ling irrigation, even in the case of their early tillage (Pratt 1961). Potter et al. (1987) reported that, conversely, the reflectance of plowed sandy soils increased by about 25% after rain and subsequent drying of their surface.

Obukhov and Orlov (1964) reported that dried unstructured soil surfaces reflected 15–20% more solar reflective radiation than similar dried soils with a well-developed structure. Van der Heide and Koolen (1980) noticed that changes in the surface structure of such soils do not modify the shape of their reflectance spectra. The reflectance level of plowed soils clearly increases after rainfall and the drying of their surface (Cierniewski 1999, 2001). Cipra et al. (1971), in analyzing spectral reflectance of *Alfisols* developed from fine loamy textures, found that wetting and drying of those soils created a thin crust on their surfaces, significantly smoothing them and increasing their reflectance. Kondratyev and Fedchenko (1980) reported that the crust created on soils with aggregates and clods with a diameter of 5 to 15 cm increased the reflectance of the soils by 10–15%. The authors also explained that the lightening of surface of these soils could be the effect of washing out the clay and humus fractions from the surface of the aggregates and clods, which could significantly increase the share of bright quartz particles on their surface. Other authors—Ben-Dor et al. (2003), Eshel et al. (2004), Goldshleger et al. (2004), and de Jong et al. (2011)—estimated that this increase in the spectral reflectance caused by the crust ranged from 10 to 40%.

2.4 Measurements of Soil Bidirectional Reflectance

Most of the goniometric devices for testing the bidirectional reflectance of soil samples in the laboratory are equipped with one collimated halogen light source that can change its zenith angle being invariably aimed at the center of these samples and not changing distance from them. Devices of a similar purpose working in field conditions use the natural illumination of direct sunbeams (reaching the tested surfaces under the changing zenith and azimuth angles) with different share of the diffuse skylight. In both cases, the bidirectional reflectance of soil surfaces, such as others, is measured from many directions, and expressed using BRF or HDRF, where measurements of the radiant flux reaching the tested surfaces are determined by measuring the radiant flux reflected from the ideal lossless Lambertian panel. The majority of goniometric devices operating in the laboratory are those whose sensors are always aimed at the center of the samples and the panel, regardless of the direction of their observation. Examples of such devices are: a compact laboratory spectrogoniometer (CLabSpeG) developed at the Katholieke Universiteit Leuven, Belgium (Biliouris et al. 2007), University of Lethbridge Goniometer System 2.0 (ULGS-2.0) constructed in Canada (Coburn and Peddle 2006), Goniometer of Rochester Institute of Technology (GRIT) made in USA (Bachmann et al. 2017; Harms et al. 2017). Some of the goniometers specially designated for field measurements observe the tested surfaces in the same way as those mentioned above. The most well-known are the Field Goniometer System (FIGOS) developed by the Remote Sensing Laboratory of the University of Zurich and the Sandmeier Field Goniometer (SFG) by the NASA Ames Research Center (Sandmeier 2000). NASA has also constructed a field Portable Apparatus for Rapid Acquisition of Land and Atmosphere (PARABOLA) that observes studied surfaces differently (Deering et al. 1990). The goniometer's boom-mounted rotating head, which changes the view zenith angle (θ_v) of the surfaces along a direction expressed by the azimuth angle, aims its sensor at other adjacent surface fragments.

2.5 Modeling of Soil Bidirectional Reflectance

The influence of soil surface roughness, illumination and viewing conditions of soils on the soil bidirectional reflectance pattern that are discussed on the above examples is better understood if it is modeled mathematically.

Walthall et al. (1985) express bidirectional reflectance of a bare soil surface as a three-parameter function of view direction to the solar direction. These parameters of an empirical character are not explicitly related to soil surface properties.

The model by Norman et al. (1985) was worked out on the assumption that the shadowing of larger soil particles or aggregates, which are simulated by cuboids, has a greater influence on the soil reflectance distribution than the scattering properties of basic soil particles of silt and clay. The cuboids and horizontal surface on which

they lie have Lambertian scattering properties. Soil surfaces simulated in this way show a backscatter regime. The bidirectional reflectance distribution function for the simulated soil surface shows a clear backscatter regime. It manifests higher reflectance if the Sun is at the 'back' of the sensor. The reflectance peak increases with the increase in the solar zenith angle. For nearly smooth soils, the distribution is almost quite 'flat', and the soil surface behaves as a perfect Lambertian reflector.

The Monte Carlo soil surface reflectance model created by Cooper and Smith (1985) was developed to study the effects that bare soil surface irregularities much larger than the wavelength of incident radiation had on soil reflectance. It assumes that the soil is a perfectly diffuse reflector at a microscopic level. So, the probability that a photon will be scattered at a given angle only depends on the orientation of the soil surface irregularities. They are described by two microrelief forms whose heights vary periodically with cosine in one or two directions for 'row' and 'clump' soils respectively. The diffuse character of the model causes rough soil surfaces to show the backscattering regime.

Models Hapke's (1981, 1984, 1986, 1993, 2002, 2008) models developed for interpreting the reflectance properties of planetary surfaces produce bidirectional signatures similar to those of a medium composed of particles characterized by a single scattering albedo and a phase function. The models take into account a parameter that depends upon regolith porosity and particle size distribution. They are applicable to macroscopically rough surfaces, i.e., those with irregularities at scales larger than the wavelength of the radiation interacting with them. The macroscopic roughness causes shadowing at large phase angles and interparticle shadow hiding at small phase angles. The models have input parameters related to a single scattering coefficient, hot spot phenomenon, and the scattering phase function. Jacquemoud et al. (1992) added a specular contribution and separated those parameters that depend on the wavelength (the single-scattering albedo) from those that were not wavelength-dependent.

The model by Irons et al. (1992) describes the soil surface as being made of uniform opaque spheres regularly spaced on a horizontal surface. The geometry of the structure (roughness) is defined as the area of a single sphere in the horizontal projection in a circle of unit area of the horizontal surface. Both direct and isotropically diffuse light illuminate the soil surface. The spheres and background are Lambertian. Soil reflectance is expressed as a function of the horizontal area shaded by the spheres, the sunlit fraction, and the proportion of diffuse illumination, which depends on wavelength. These terms depend on the solar and view directions and on the characteristics of the simulated surface. The model uses an empirical function describing the relation between the fractional area of the plane in which shadow area overlaps the area obscured from view by the sphere, and the angle between the directions of solar illumination and viewing. The model was fit to soil bidirectional reflectance data for bare loamy soil of varying surface roughness.

Otterman's model (Otterman 1981, 1985; Deering et al. 1990) treats bare soil as thin vertical cylinders of variable heights with facet-reflectance and transmittance located randomly on a horizontal plane with Lambertian reflectance. The architecture of the soil protrusions is described by a parameter, which is the sum of the

height times diameter of these cylinders per unit horizontal area. The model assumes that the facet-reflectance largely controls the backscatter while facet transmittance is responsible for determining forward scattering. This was the first model simulating both backscattering and forward scattering. It predicted a clear forward scattering character of reflectance for a surface with nearly pure gypsum crystals of high transmittance.

The first model of Cierniewski (1987, 1988, 1989) describes soil aggregates by regularly spaced equal-sized opaque spheres of a given diameter. This first model takes into account a freely sloping plane at a specified angle on which the aggregates are lying. The roughness of the geometrical structure is expressed as the proportion of the areas of aggregates (in the plane parallel to the soil sloping plane) in a given unit area of soil surface. Sunbeams illuminate this structure at θ_s. A part of it is shaded. It is assumed that the reflectance level of a rough soil surface in relation to a soil that is the same but for having a smooth surface decreases with an increase in the share of shaded fragments of this structure according to the exponential function. Successively improved versions of the model simulate soil aggregates by spheroids with a specific ratio of their vertical to horizontal radii (Cierniewski and Verbrugghe 1993), the structure of simulated soil surface being illuminated both by direct sunbeams and by diffuse light expressed by a specified factor (Cierniewski and Verbrugghe 1994), and the radiation leaving the fragments directly illuminated by sunbeams having a specular-diffuse character (Cierniewski et al. 1996; Cierniewski and Verbrugghe 1997a, 1997b). This reflected radiance in these versions of the geometrical model is expressed by the relative reflectance factor defined as the proportion of the total radiance viewed from the off-nadir direction to the radiance viewed from the nadir.

The next model also predicts the distributions of shortwave radiation reflected from soil surfaces, the irregularities of which are caused by soil particles and aggregates dispersed regularly in all directions (Cierniewski 1999). The model calculates the directional reflectance of such soil surfaces along the solar principal plane (SPP), where the variation of the reflectance in θ_v is the highest. Using the fact that the reflectance variation at the orthogonal plane (OP) is minimum near zero, the model also approximates this reflectance distribution at any measure plane outside of the SPP, interpolating it between the SPP and OP planes. Soil aggregates in this model have a more realistic shape than the model discussed above. The soil surface is simulated by equal-sized opaque spheroids with horizontal (a) and vertical (b) radii lying on a freely sloping plane at angle β (Fig. 4). They are absorbed into the ground of the slope plane, having their tops at height t above the ground. The spheroids are regularly arranged on the slope plane so their centers are in a net of squares of the side d. The model was tested in outdoor conditions on soil samples formed by: dune sand (with particles of 0.05 cm diameter) and loamy sand to sandy loam materials with aggregates of diameter from 1.5 cm to 4 cm, as well as stones with diameter of 5–6 cm and loamy clods simulating their general shape. Figure 5 shows photography of the dune sand, and its synthetic surface that enables the generation of its normalized reflectance (NR) distribution along the SPP for 0.65 μm. The distribution reveals the impact of specular features of the sand in the forward scattering direction particularly at high θ_s angles. The next figures show analogous data for cultivated rough

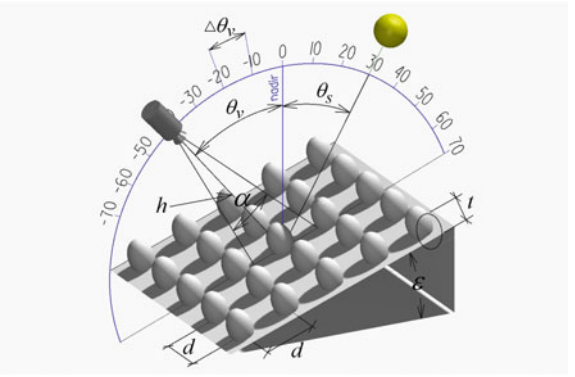

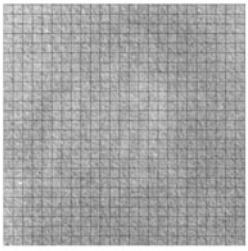

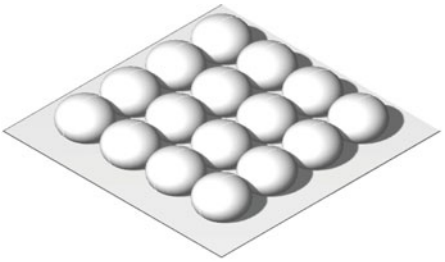

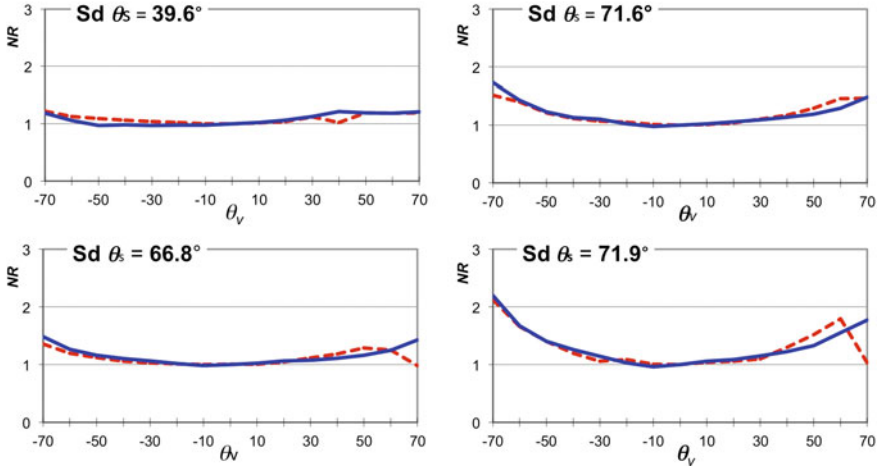

Fig. 4 Illumination and viewing geometry of the soil surface representation in the model of Cierniewski (1999)

Fig. 5 Photography of the dune sand (Sd), its synthetic surface and normalized reflectance (*NR*), measured (red dashed line) and predicted (blue solid line) along the solar principal plane illuminated at different solar zenith angles (θ_s) for the wavelengths of 0.65 μm

and smoothed soils developed from loamy sand (Fig. 6) and sandy loam (Fig. 7). The higher the θ_s, the greater the *NR* variation of these surfaces along the SPP, regardless

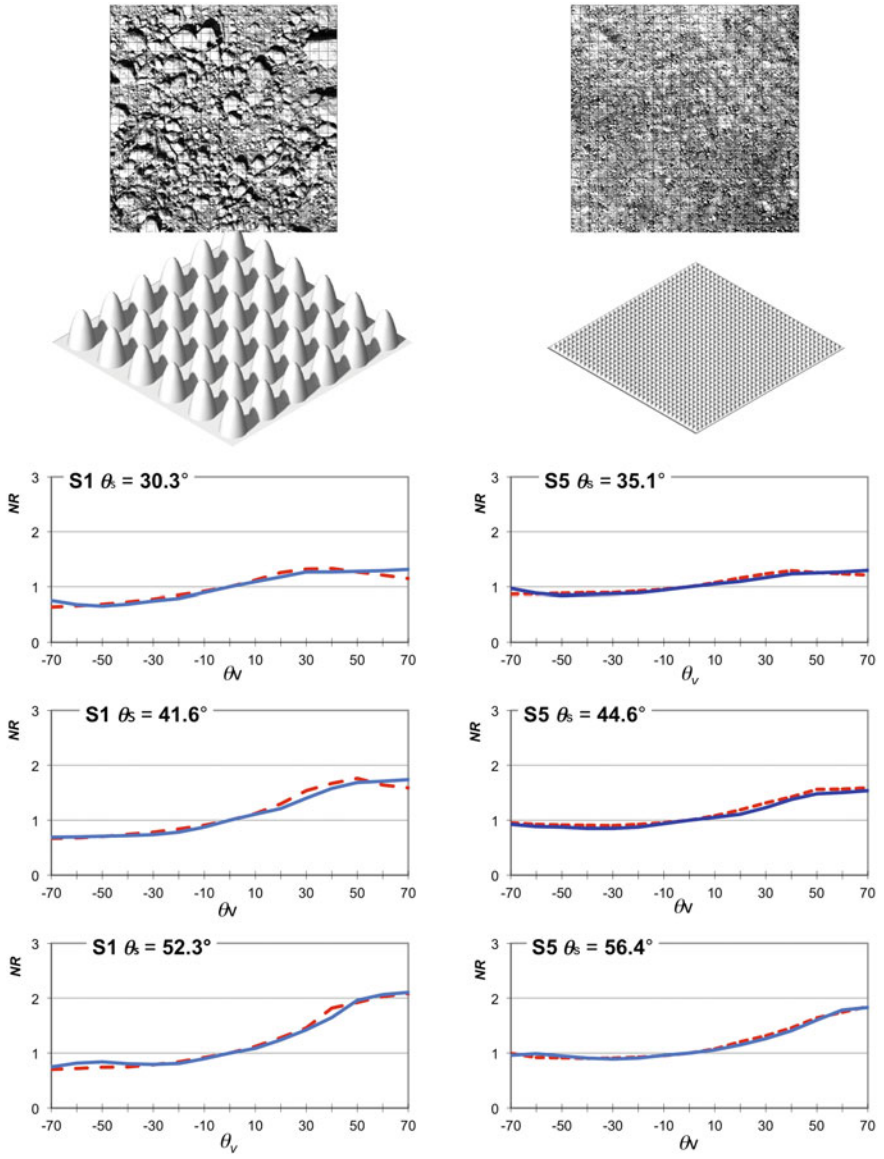

Fig. 6 Photographs of cultivated rough (S1) and smoothed (S5) loamy sands and their synthetic surfaces with their normalized reflectance (*NR*), measured (red dashed line) and predicted (blue solid line) along the solar principal plane illuminated at different solar zenith angles (θ_s) for the wavelengths of 0.65 μm

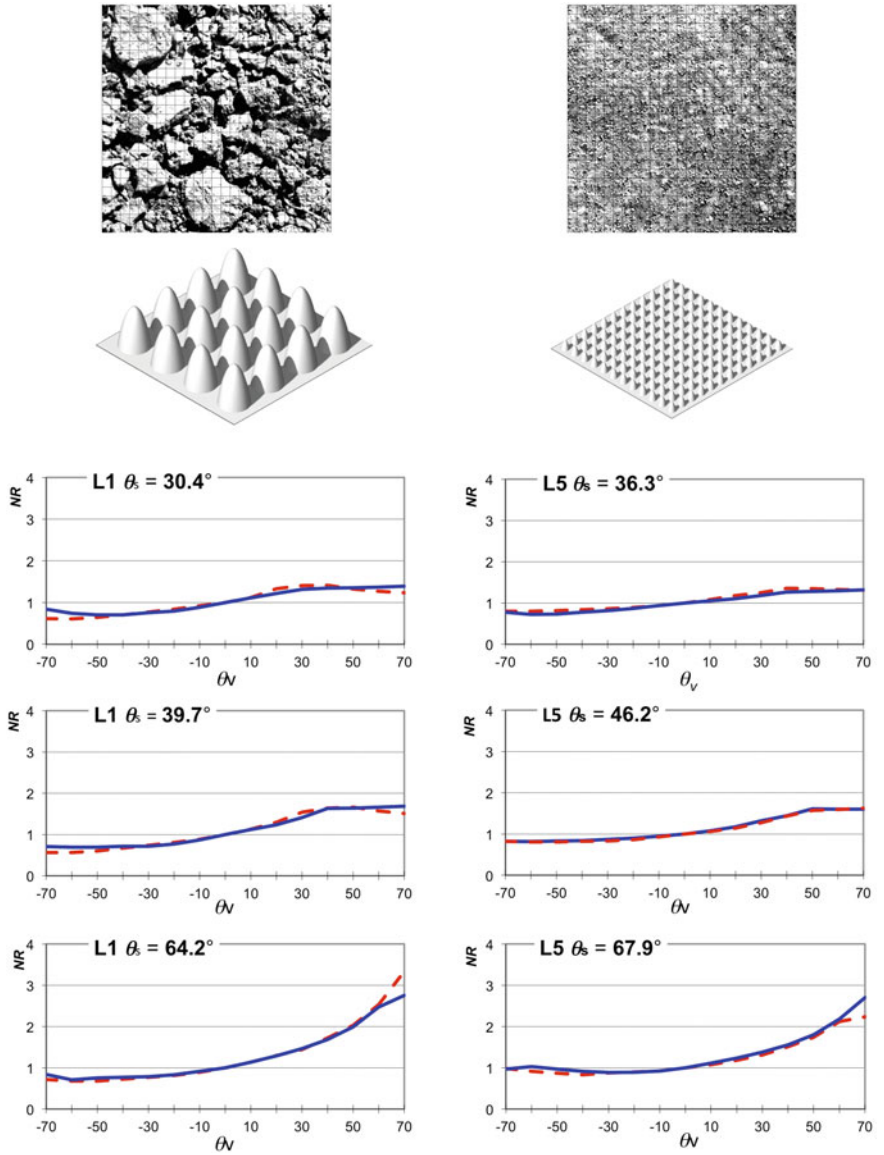

Fig. 7 Photographs of cultivated rough (L1) and smoothed (L5) sandy loams and their synthetic surfaces with their normalized reflectance (*NR*), measured (red dashed line) and predicted (blue solid line) along the solar principal plane illuminated at different solar zenith angles (θ_s) for the wavelengths of 0.65 μm

of their roughness. The effect of the specular component in the *NR* data of both cultivated soils is almost invisible. In contrast, the increasing variation of their *NR* along the SPP as a result of their smoothing is clearly visible. The data presented in Fig. 8, which show surfaces of a similar general shape made of stones and loamy clods, prove that their spectral reflectance is determined more by this shape than by their texture.

The model published two years later (Cierniewski 2001) describes the spectral reflectance from soil surfaces subjected to directional agricultural treatments (Fig. 9). Simulated soil aggregates are spread on such surfaces in a row, creating furrows of a kind along the direction of these treatments. The spheroids are situated on planes described by the vertical angle β_{d} related to the plane of the horizon and the horizontal angle $\phi_{\mathrm{d\text{-}s}}$ determined in relation to the direction of the sun's rays. The slope represents two parallel planes: the lower one, which is defined by the lines running in the bottom of the hollows between the furrows, and the above-laid plane constituting the base of the ridge of these furrows. The horizontal angle between these lines and the direction of sunlight $\phi_{\mathrm{c-s}}$ determines the direction of the agricultural treatments. The spheroids are pressed into the upper plane, so that their tops protrude above it to a height of t_{r}. With regard to this, t_{p} specifies the irregularities of the simulated surface in the direction perpendicular to the direction of furrows. Irregularities in this surface along the direction of furrows are smaller, which is expressed by the smaller height of protruding parts of the ellipsoid t_{r} above the plane of the furrow ridge. The geometrical structures of the two above models are illuminated by direct sunbeams coming to it at θ_s, and by diffuse light described by the factor f_{di}. The f_{di} approximates a reflectance effect from soil surfaces illuminated only by the diffuse light component. The factor is defined as the part of the direct solar beams' radiation. A sensor is suspended over the simulated soil surfaces. It observes them along the SPP at zenith angles θ_v, at the $\Delta\theta_v$ increments in forward scattering and backscattering directions, which are described by negative and positive values of the θ_v, respectively. The sensor aims at the same point of the analyzed surfaces, being at distance h from it. The sensor field of view defines the angle ξ.

The reflectance of the main solar plane is calculated twice, assuming that the SPP runs along the furrows and perpendicular to this direction. The amounts of energy reaching the directly illuminated fragments of the simulated soil structure are calculated using the factor $Ei^{\downarrow}_{vfa}$:

$$Ei^{\downarrow}_{vfa} = \cos\theta_s \cos\beta_{fa} + \sin\beta_{fa} + \sin\theta_s + \cos(\phi_d - \phi_s), \tag{5}$$

where: β_{fa} is the angle of inclination of the elementary fragment of this structure, and ϕ_d and ϕ_s are the horizontal angles describing, respectively, the location of the soil slope and the Sun. The factor $Ei^{\downarrow}_{vfa}$ expresses the cosine of the angle of incidence of the rays' γ relative to the normal one for the elementary fragment *fa*. Radiation falling on the fragment is reflected in both a diffusive and a specular way, and its vectors in the two-dimensional plane create the shape of a circle and an elongated ellipse, respectively (Fig. 10). The length of the vectors of the specular component, treated as non-polarized light, is calculated using the Fresnel equations:

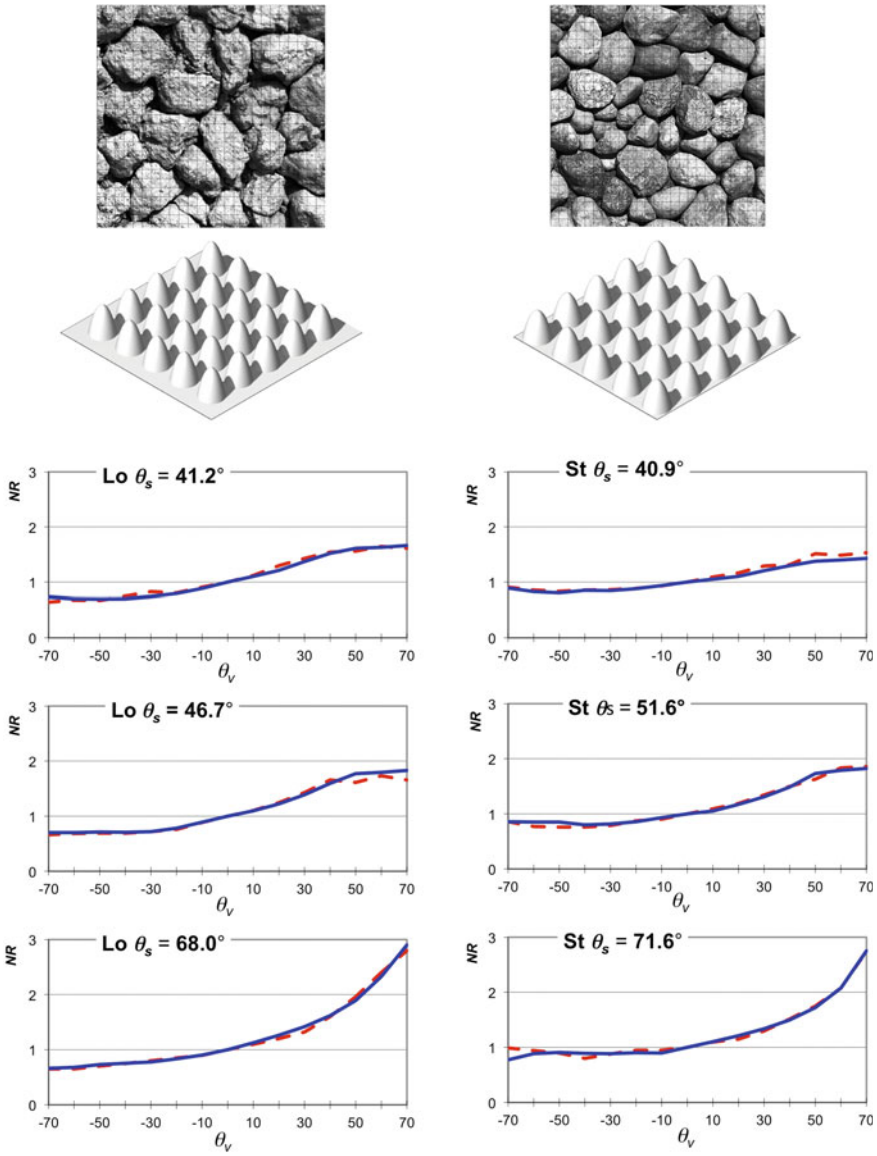

Fig. 8 Surfaces of a similar general shape made of loamy clods (Lo) and stones (St) and their synthetic surfaces with their normalized reflectance (*NR*), measured (red dashed line) and predicted (blue solid line) along the solar principal plane illuminated at different solar zenith angles (θ_s) for the wavelengths of 0.65 μm

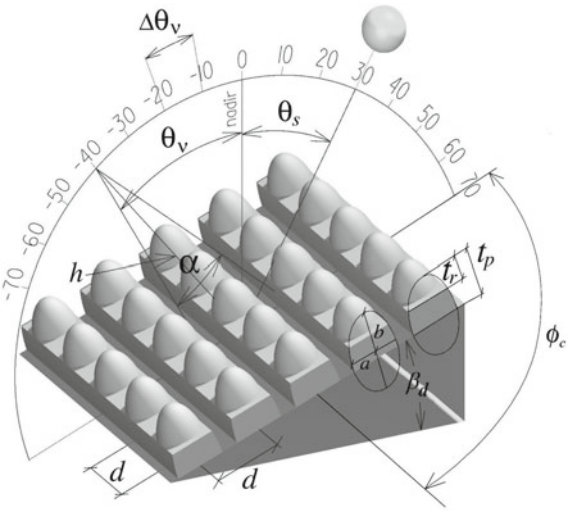

Fig. 9 Illumination and viewing geometry of a simulated soil surface with furrowed microrelief in the model of Cierniewski (2001)

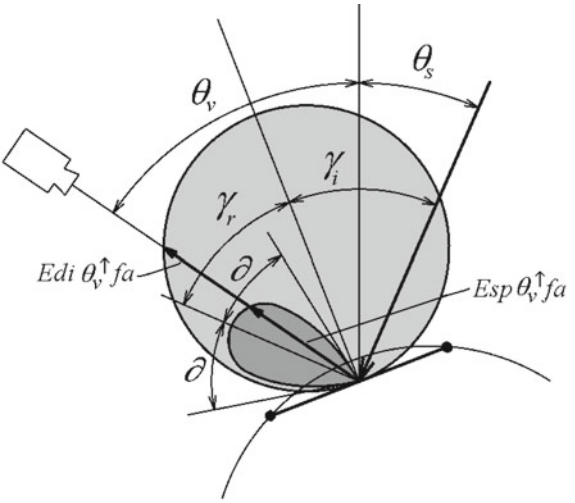

Fig. 10 Distribution of the energy leaving a facet of the simulated soil surface in the specular Esp_{vfa} and the diffuse way Edi_{vfa}

$$Esp^{\uparrow}_{\theta_v fa} = Ei^{\downarrow}_{vfa} Fp_{(\gamma_i)} \quad Fp_{(\gamma_i)} = \frac{r_{\perp}^2 + r_{=}^2}{2} \tag{6}$$

where $r_{\perp}$ and $r_{=}$ are respectively the perpendicular and parallel Fresnel reflection coefficient. The vector of reflected energy $Esp^{\uparrow}_{\theta_v fa}$ is oriented in such a way that the angle of incidence γ_{i} equals the reflection angle γ_{r}. Specular effects are perceived by the sensor only to a limited extent defined by the angle 2∂ around the direction γ_{r}. The length of the $Esp^{\uparrow}_{\theta_v fa}$ vector at a distance $\pm\partial$ from γ_{r} falls linearly to zero.

The length of the vector $Ei^{\downarrow}_{vfa}$ completes the diffuse component $Edi^{\uparrow}_{\theta v\ fa}$ is defined as:

$$Edi^{\uparrow}_{\theta_v fa} = \left(1 - Fp_{(\gamma_i)}\right) Ei^{\downarrow}_{vfa} \cos\theta_v. \tag{7}$$

Finally, the total radiation $Eis^{\uparrow}_{\theta_v fa}$ reaching to the sensor at θ_v, reflected from the directly illuminated elemental part *fa* of simulated soils is calculated by dividing $Ei^{\downarrow}_{vfa}$ by $\cos\theta_v$. The amount of diffuse sky-light ($E^{\downarrow}_{sk\,\mathrm{fa}}$) that reaches to the sunlit and shaded fragments of the simulated soil surface is reduced by the presence of neighbouring ellipsoids (Fig. 11):

$$Esk^{\downarrow}_{fa} = f_{di}\frac{\delta}{180^{\circ}}, \tag{8}$$

where δ is a plane angle in the analyzed plane limiting the sky light input to the analyzed fragment of the simulated soil surface. The luminance factor of the simulated soil surface, including sunlit and shaded elementary fragments, viewed at θ_v along a specific profile is defined as:

$$L^{\uparrow}_{\theta_v} pr = \sum_{i=1}^{j}\left[\left(Eis^{\uparrow}_{\theta_v fa} + Esk^{\downarrow}_{fa_{(i)}}\right)\xi i_{fa_{(i)}}\right] + \sum_{i=1}^{j}\left(Esk^{\downarrow}_{fa} + \xi s_{fa_{(i)}}\right), \tag{9}$$

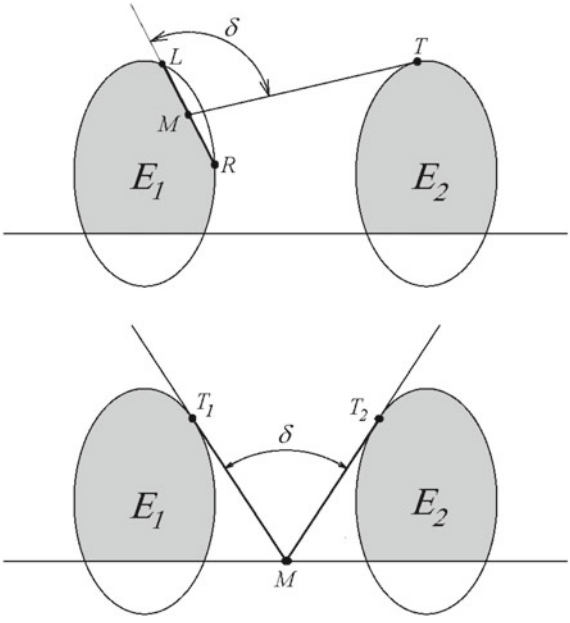

Fig. 11 Limitation in illumination by skylight of the facet segment (*LR*) on the ellipse E_1 ark and the slope plane between ellipses E_1 and E_2, expressed by the angle δ. *M* is the middle point of the segments *LR* and T_1 and T_2 are the tangent points of the angle δ sides to the adjoining ellipses

where i is the fragment of the analyzed structure, ξ_{ifa} and ξ_{sfa} are respectively elementary viewing angles of illuminated and shaded fragments. Luminance received by the sensor from its entire field of view, $L^{\uparrow}_{\theta_v FOV}$ is the average value of luminance from individual cross-sections $L^{\uparrow}_{\theta_v} pr$ and the space between ellipsoids $L^{\uparrow}_{\theta_v} sm$, weighted according to the equation:

$$L^{\uparrow}_{\theta_v FOV} = L^{\uparrow}_{\theta_v} pr_{(1)} \frac{a}{2\mathrm{m}-1} + \sum_{i=2}^{m} L^{\uparrow}_{\theta_v} pr_{(i)} \frac{a}{m-0.5} + L^{\uparrow}_{\theta_v} sm\left(\frac{d}{2} - a\right), \quad (10)$$

where m is the number o the profiles. If modeling directional spectral reflection is to refer to a situation where the main solar plane does not run either parallel or perpendicular to the direction of fissures, then the luminance $L^{\uparrow}_{(\phi_r,\theta_v)FOV}$ of the illuminated surface is calculated according to the equation:

$$L^{\uparrow}_{(\phi_r,\theta_v)FOV} = Lr^{\uparrow}_{\theta_v, FOV}\left(1 - \frac{\psi}{90^{\circ}}\right) + Lp^{\uparrow}_{\theta_v, FOV}\frac{\psi}{90^{\circ}}, \quad (11)$$

where $Lr^{\uparrow}_{\theta_v, FOV}$ and $Lp^{\uparrow}_{\theta_v, FOV}$ are luminance values calculated respectively along and perpendicular to the direction of furrows, and ψ is the horizontal angle measured between the SPP and the direction of the furrow course. Finally, reflectance from the rough surface of the soil along the SPP is described by means of the normalized indicator $NR_{(\theta_v=\mathrm{SPP},\theta_v)}$, defined as the ratio of total luminance $L^{\uparrow}_{\theta_v FOV}$ of the soil surface measured obliquely to its luminance measured in the nadir direction. Assuming that the NR index in the OP for each angle θ_v takes the value 1, the distribution of $NR_{(\phi_v,\theta_v)}$ in the function of the azimuthal angle ϕ_v between SPP and OP has a straight line and its value for any oriented plane can be defined as:

$$NR_{(\phi_v,\theta_v)} = NR_{(\theta_v=\mathrm{SPP},\theta_v)} + \left(1 - \frac{\phi_v}{90^{\circ}}\right) + \frac{\phi_v}{90^{\circ}}, \quad (12)$$

where ϕ_v is the relative horizontal angle determining the angular distance from the SPP. The model was tested in field conditions on plots with loamy sand and sandy loam soils freshly formed by a plow and harrows and then modified by rainfalls in Poland (Cierniewski 2001), on fields in France with a loamy soil that had been plowed, harrowed and rolled, and prepared for sowing colza (Cierniewski et al. 2002). The irregularities in the plots tested in Poland were recorded on stereoscopic images. The maximum difference in height of the presented fragment of the freshly plowed field was 35 cm (Fig. 12) and, after a total of 92 mm rainfall, was only 26 cm (Fig. 13). The larger height differences were observed transversely, rather than along the furrows. The standard deviation of the height crosswise and parallel to the furrows were 4.6 and 4.4 cm, respectively, in the first case, and 1.9 and 1.5 cm in the second. In the freshly plowed surface, larger aggregates that had previously had sharp edges changed their shape to round after this rainfall, and the smaller soil aggregates were mostly eliminated. The height difference in the same surface developed from the

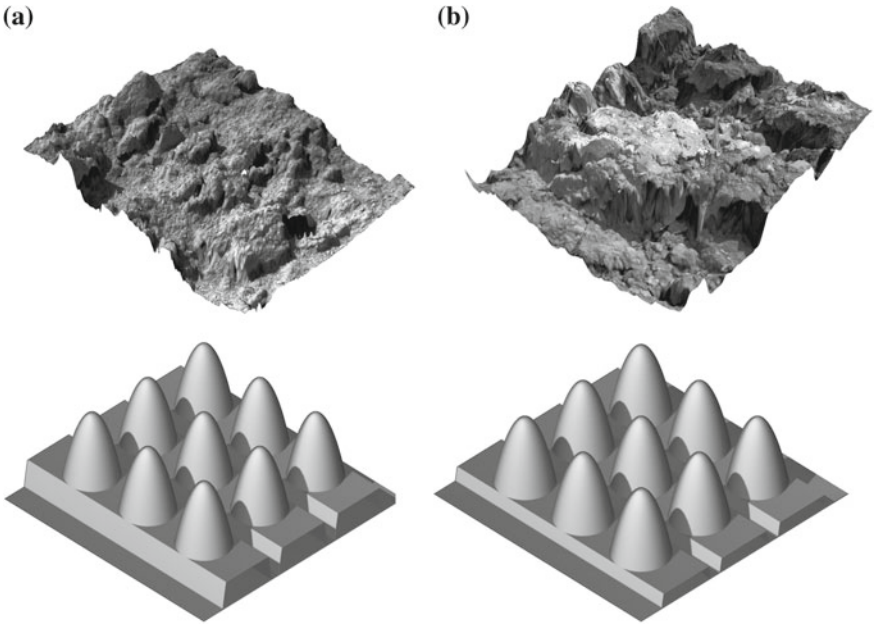

Fig. 12 View of soil surfaces 50 × 50 cm size, freshly plowed (**a**) and after 92 mm (**b**) with their diagrams of digital elevation model in the form of a triangular net covered by the real image and below their virtual equivalents

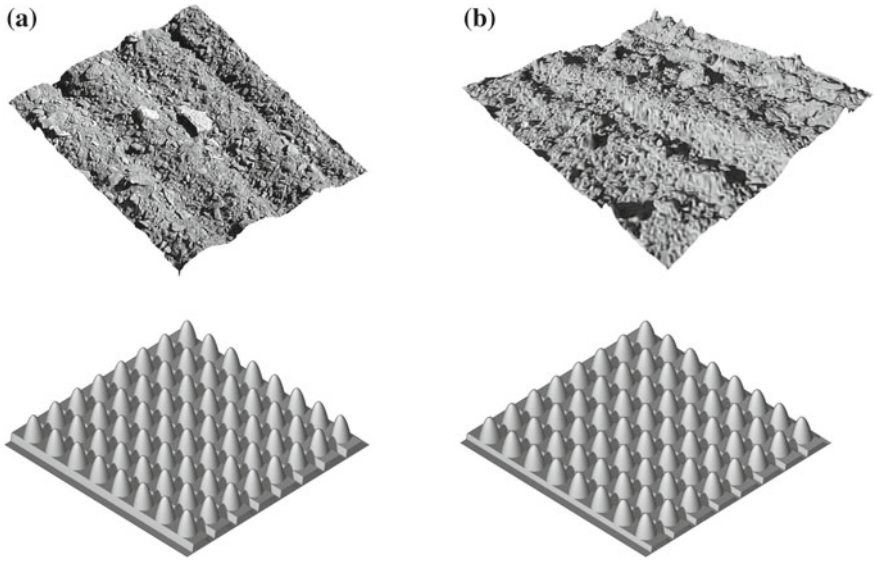

Fig. 13 View of soil surfaces 50 × 50 cm size, freshly harrowed and after 25 mm rain **a** with their diagrams of digital elevation model in the form of a triangular net covered by the real image and below their virtual equivalents

loamy sand reached 10 cm, and 7 cm after a total of 25 mm rainfall. The standard deviation of its height both crosswise and parallel to its furrows was 1.3 cm for the freshly formed surface and 1.2 cm after the rainfall. The measured and predicted data using this model show that the *NR* variation of these plots increased along the SPP due not only to the increase in θ_s, but also to the increase in ϕ_{c-s} angle describing the illumination of their furrows. This variation is the greater, the deeper their furrows. This is particularly evident in the case of plots illuminated at almost the same θ_s angles. Thus, the impact of this ϕ_{c-s} is more pronounced for freshly plowed plot (Fig. 14) than harrowed plots (Fig. 15) and it becomes less visible due to the gradual smoothing of the surface of larger soil aggregates by rain (Fig. 16) and complete elimination of smaller aggregates (Fig. 17). It should also be noted that the measured reflectance of the soils (in the diagrams expressed by its *BRF* and marked with the '*R*' symbol) are clearly lower for plots with greater roughness, i.e. with deeper freshly formed furrows than those with lower roughness, especially with those modified after rainfall. The reflectance of soils used to test this model was measured in Poland by a six-channel field luminancemeter in the following wavelength bands: 0.45, 0.55, 0.65, 0.85 and 1.65 μm, and in France by three channel bands: 0.55, 0.65, 0.85 μm. The soil reflectance data collected in France show that rougher soil surfaces do not always have a higher variation in *NR* distribution along the SPP than do smooth

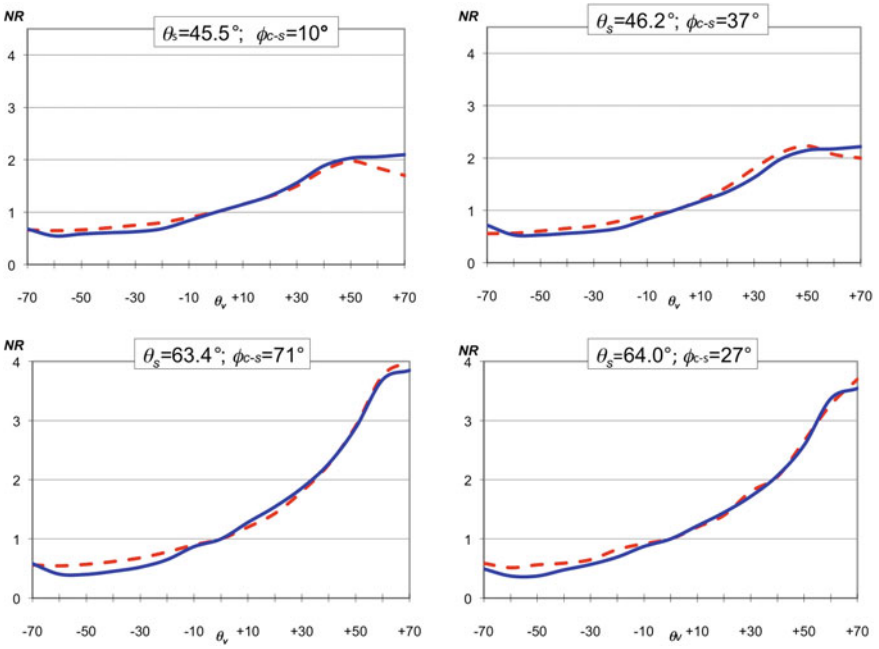

Fig. 14 Normalized reflectance (*NR*), measured (red dashed line) and predicted (blue solid line) of freshly plowed plots illuminated at almost the same θ_s and different ϕ_{c-s} angles along the solar principal plane, for the wavelengths of 0.85 μm

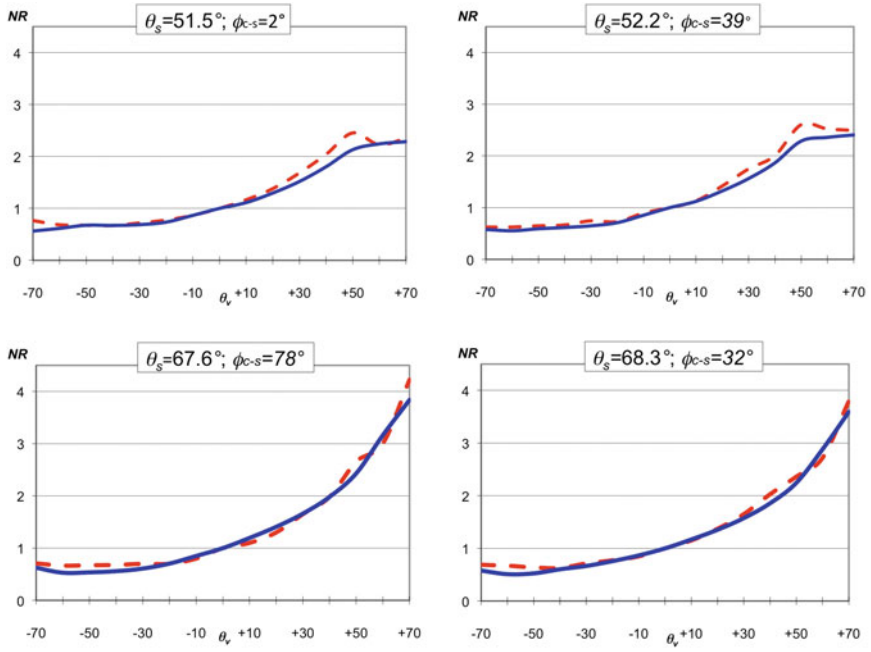

Fig. 15 Normalized reflectance (*NR*), measured (red dashed line) and predicted (blue solid line) of freshly harrowed plots illuminated at almost the same θ_s and different ϕ_{c-s} angles along the solar principal plane, for the wavelengths of 0.85 μm

ones. Soil surfaces smoothed by rolling can display an *NR* distribution quite similar to those of more rough surfaces that have been ploughed or furrowed by a seeder (Fig. 18).

The distribution of hemispherical-directional reflectance of cultivated and uncultivated soils was also modeled by surfaces with irregularities constructed by a set of n points k_i of coordinates (x_i, y_i, z_i) of $i = 1, \ldots, n$ and the positive real numbers r_1, r_2, r_3, …, r_n related to them, respectively (Cierniewski et al. 2004). A pair (k_i, r_i) is interpreted as the opaque sphere of radius r_i with the center k_i. The shape of those surfaces is the solution of the following equation:

$$\sum_{i=1}^{n}\left(2d_i^3 - 3d_i^2 + 1\right) - \frac{1}{2} = 0 \quad d_i = \frac{\min\left(r_i\sqrt{(x-x_i)^2 + (y-y_i)^2 + +(z-z_i)^2}\right)}{r_i} \tag{13}$$

The centers k_i are dispersed regularly in a net of squares with a side of $1/\sqrt{n}$ in the perpendicular projection to the XY plane. The height z_i of the k_i center is expressed by the equation:

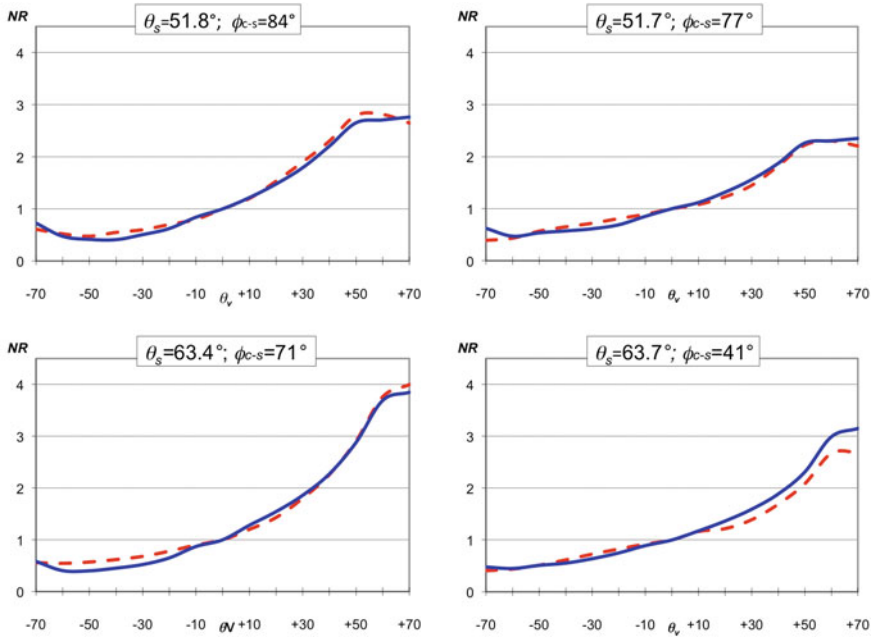

Fig. 16 Normalized reflectance (*NR*), measured (red dashed line) and predicted (blue solid line) of plowed plots after smoothing them by 92 mm rainfall illuminated at almost the same θ_s and different ϕ_{c-s} angles along the solar principal plane, for the wavelengths of 0.85 μm

$$z_i = a \cdot |\sin(\pi \cdot x_i)| \cdot \langle 1 - b \cdot [1 - |\sin(\pi \cdot y_i)|] \rangle + c \cdot f_{dis}(i), \tag{14}$$

where a expresses the amplitude of sin function along the x-axis, and b along the y-axis to a. The final z_i position of ith sphere is an effect of a disturbance approximated by the sequence $f_{dis}(i) \in [0.1)$ with uniform distribution. The c describes the maximum deviation from the z_i value, as determined by only these a and b parameters (Fig. 19). The shape of the surface is characterized by the directivity factor D_R, expressing the differences between the maximum and the minimum deviations of its height, calculated along all possible directions (Fig. 20).

The surface is illuminated by a hemisphere light source created by m point sources $s_1, s_2, s_3, \ldots, s_m$ of the intensity $e_1, e_2, e_3, \ldots, e_m$, respectively, equally spread on the hemisphere. It is assumed that in outdoor conditions the ratio of the direct solar irradiance to the global irradiance δ in clear-sky conditions changes with the sun's position $S = [\theta_s, \phi_s]$ and normal optical thickness τ (Fraser 1975). The distribution of the hemispherical light for the non-absorbing Rayleigh atmosphere dependent on θ_s and τ attributed to the wavelength λ is shown in Fig. 21. The intensity of the direct solar irradiance at point S reaches 1 independently of both τ and λ. The light is scattered from the simulated surface in accordance the quasi-Lambertian function (Fig. 22). The shape of the surface R described by Eq. 13 allows definition of the vectors of the normal to any points on this surface. These vectors make it possible

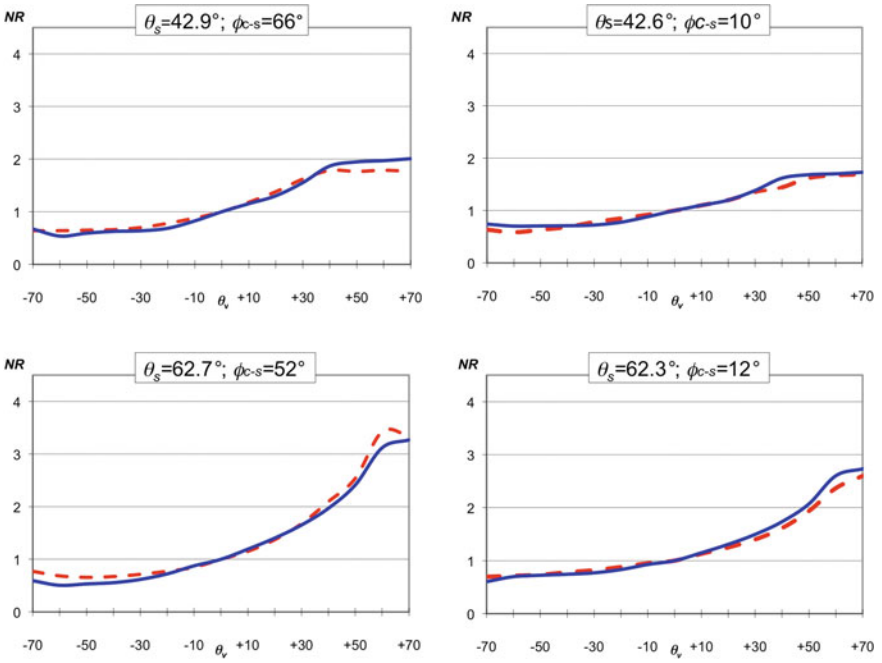

Fig. 17 Normalized reflectance (*NR*), measured (red dashed line) and predicted (blue solid line) of harrowed plots and after smoothing them 25 mmm rainfall illuminated at almost the same θ_s and different ϕ_{c-s} angles along the solar principal plane, for the wavelengths of 0.85 μm

to determine the amount and direction of the light reflected from the total area of the surface. The light $e_{f_R}\left(i, \vec{k}\right)$ reflected only once from the fragment f_R along the direction $\vec{k}$, due to illumination from the unblocked point source, s_i, is calculated as:

$$e_{f_R}\left(i, \vec{k}\right) = e_i \cdot f\left(\vec{s_i}, \vec{n}, \vec{k}\right), \tag{15}$$

where $\vec{n}$ is the normal to the fragment f_R. A cloud of all the vectors $\vec{k} \cdot e_{f_R}\left(i, \vec{k}\right)$ characterizes the scattering properties of the R surface in its f_R fragment. The total light energy $E\left(f_R, \vec{v}, H\right)$ reflected from the f_R fragment in the direction $\vec{k}$ and viewed along a direction $\vec{v} = [\theta_v, \phi_v]$ is expressed by:

$$E\left(f_R, \vec{v}, H\right) = \sum_{i=1}^{m} e_{f_R}\left(i, \vec{v}\right), \tag{16}$$

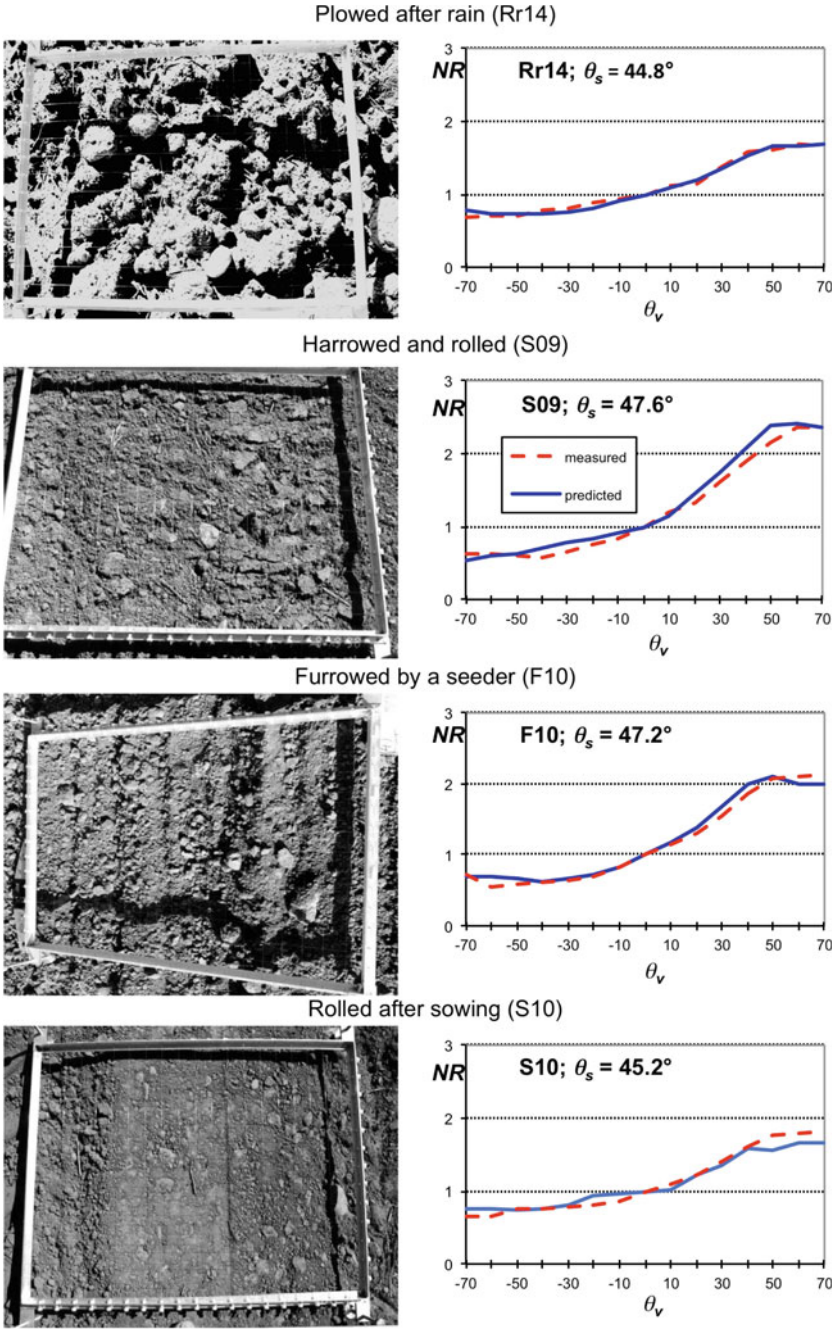

Fig. 18 View of selected soil surfaces treated by different agricultural tools with the normalized reflectance (*NR*) of the surfaces, measured and predicted by the model of Cierniewski (2001), illuminated at similar θ_s angles along the solar principal plane for the wavelength of 0.65 μm

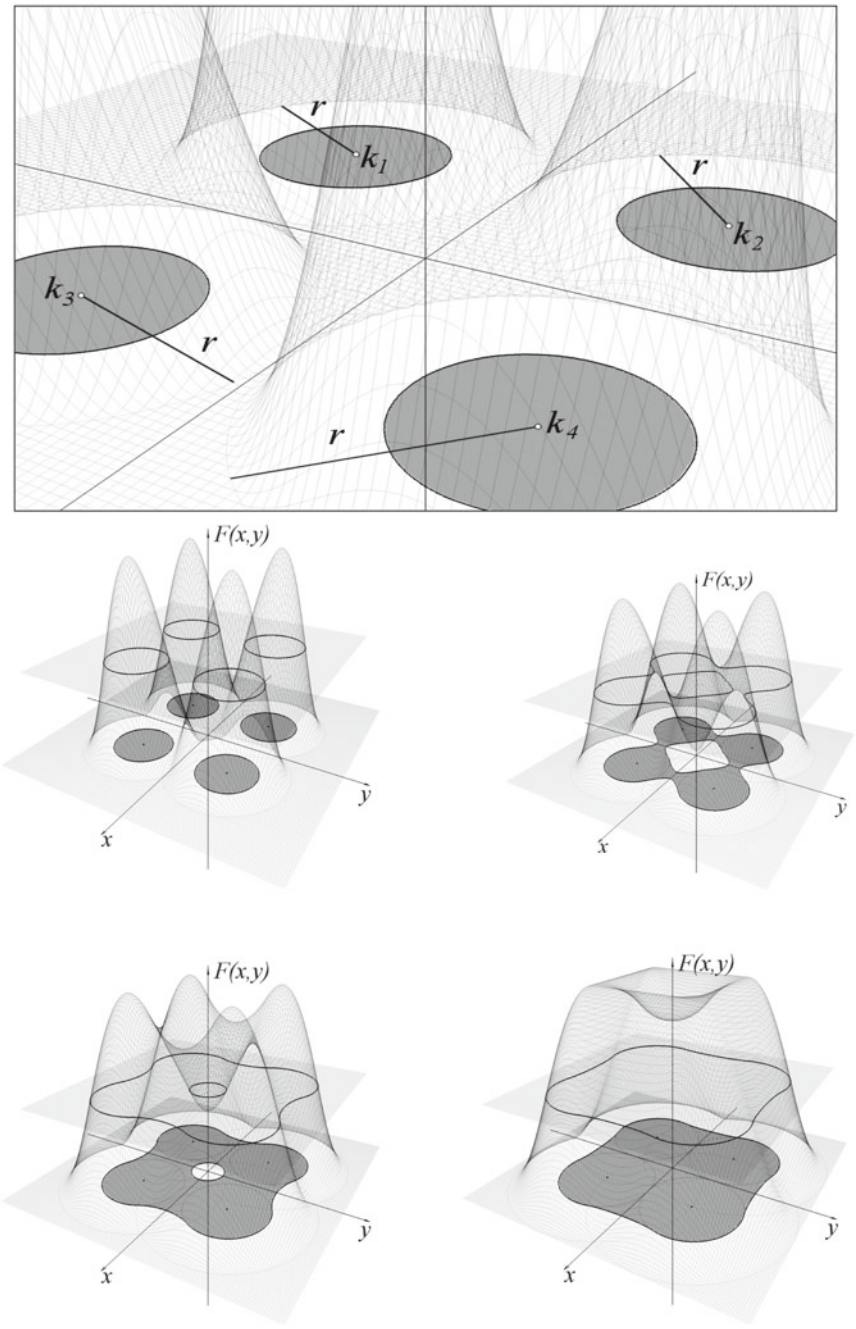
r
k1
r
k2
k3
r
r
k4
F(x,y)
y
x
F(x,y)
y
x
F(x,y)
y
x
F(x,y)
y
x

◀**Fig. 19** Influence of the radius r_i on the shape of the R surface described by Eqs. 13–14 in two dimensional space. The marked fragments on the plane OXY expresses the solutions of the equations. The higher r_i values around the points of k_i with their invariable position, the larger merging of the R shape with simultaneous reduction or elimination of gaps in it. Below—segments of soil surfaces generated by different values of the a, b, and c parameters and their directivity factors D_R

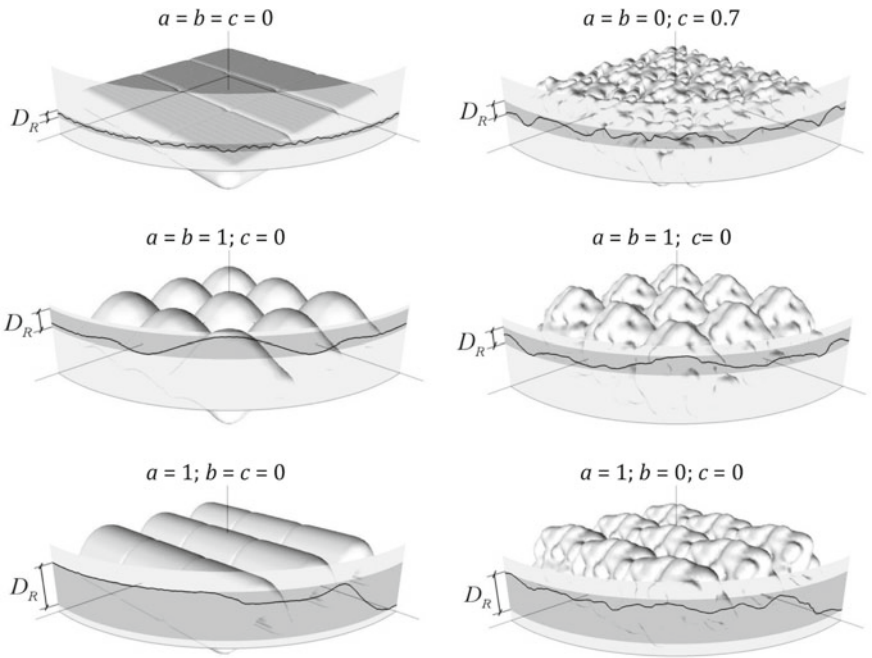

Fig. 20 Segments of soil surfaces generated by different values of the a, b, and c parameters and their directivity factors D_R

where the sum is only limited for unblock light source s_i. The function HDRDF $\left(R, \vec{v}, H\right)$:

$$\text{HDRDF}\left(R, \vec{v}, H\right) = \frac{1}{|\Omega|} \int_{\Omega} E\left(f_R, \vec{v}, H\right) d\Omega \tag{17}$$

describes the hemispherical–directional reflectance of the whole surface R, where Ω is the FOV of a sensor suspended over the surface. This model was tested on directional reflectance data collected on a bare arable soil with furrows and desert loess and rocky surfaces in Israel. They were obtained by the same six-channel luminancemeter as mentioned above. The *NR* distribution of the cultivated soil was predicted by a virtual surface with furrows as in reality. The measured *NR* values of

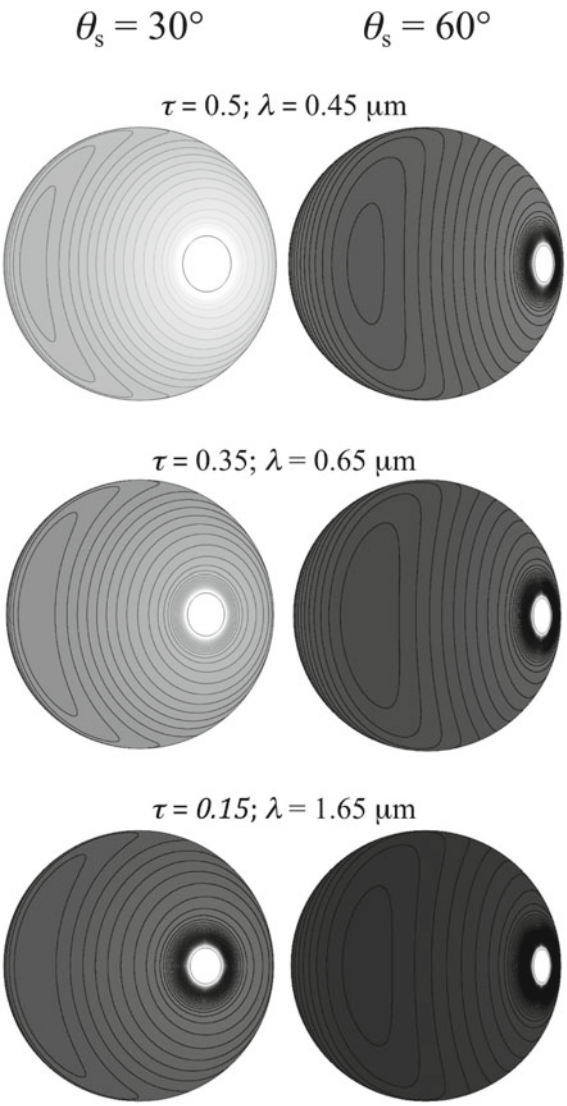

Fig. 21 Distributions of the hemispherical light for the non-absorbing Rayleigh atmosphere depending on the solar zenith angle θ_s and the normal optical thickness τ attributed to the wavelength λ

the cultivated soil, unlike its modeled values, clearly showed asymmetry in their *NR* distribution. These desert surfaces did not reveal this asymmetry either in the data measured or in the data calculated using this model (Fig. 23).

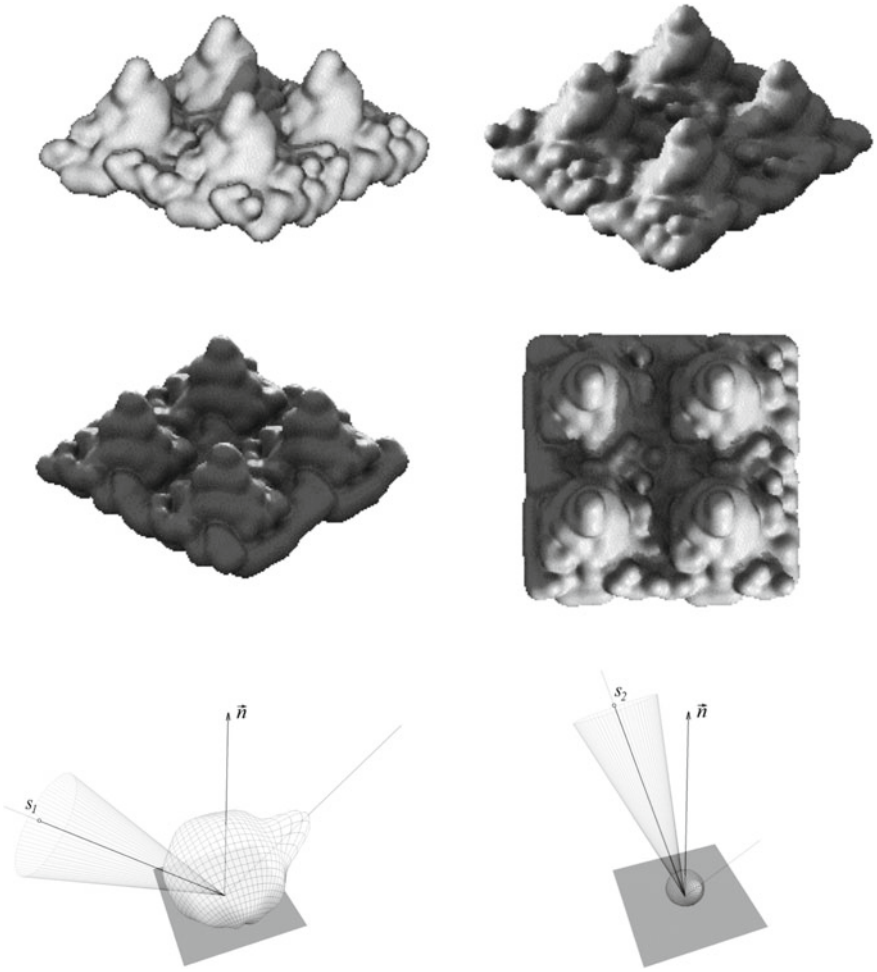

Fig. 22 Brightness variation of a soil surface illuminated unequally with one source of the dominant intensity with reference to others scattered in accordance the quasi-Lambertian function. Below—distribution of light energy coming from sources S_1 and S_2 of the intensity $e_1 > e_2$, respectively, scattered from an elementary fragment f_R of the R surface

3 Soil Albedo

If the bidirectional reflectance is only a part of the reflected radiation from a surface along a given direction, then the albedo of the surface, also called its bihemispherical reflectance (BHR):

$$\mathrm{BHR} = \rho(\theta_i, \phi_i; 2\pi; 2\pi) = \frac{d\Phi_r(\theta_i, \phi_i, 2\pi; 2\pi)}{d\Phi_r^{id}(\theta_i, \phi_i, 2\pi)} \tag{18}$$

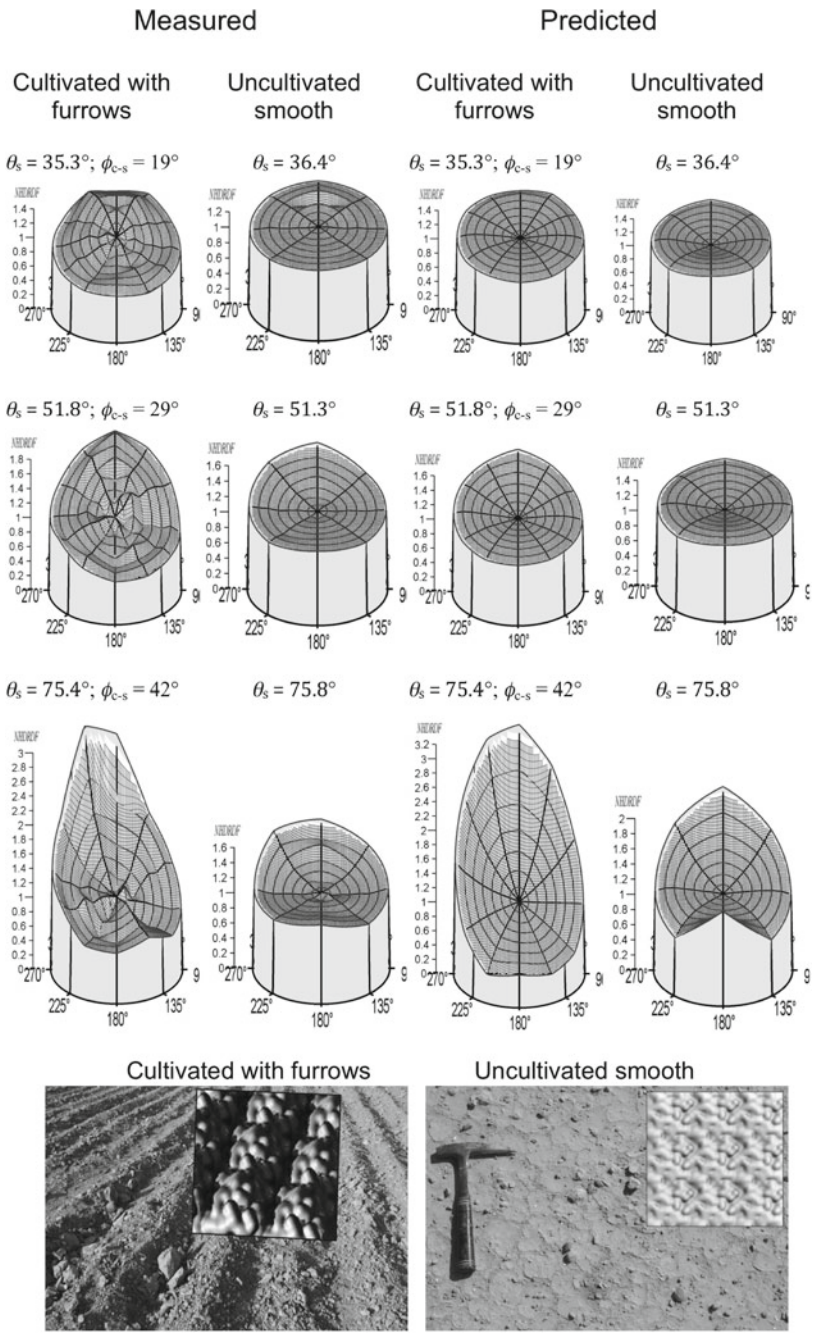

Fig. 23 Distributions of the normalized hemispherical-directional reflectance function of the tested surfaces (cultivated with furrows and the uncultivated relatively smooth), measured and generated for the wavelengths of 0.85 μm for selected illumination conditions defined by the solar zenith angle θ_s and the angle ϕ_{c-s} describing a distance angle between the direction of the furrows and the sun position. Below—view of the surfaces with their virtual equivalents

is influenced by the combined diffuse and direct irradiance and integrates the surface reflectance over all view directions. The albedo is precisely defined as the ratio of the radiant flux reflected from a unit surface area into the whole hemisphere to the incident radiant flux of hemispherical angular extended in the solar reflective radiation range of 0.3–3 μm (Schaepman-Strub et al. 2006). Martonchik et al. (2000) emphasized the distinction between the terms "broadband albedo" and "narrowband (spectral) albedo" depending on whether the albedo is characterized by the entire wavelength range or only a part of it, respectively. The blue-sky albedo refers to the albedo measured in outdoor conditions, where a surface is illuminated by the direct solar irradiance and diffuse irradiance scattered by the atmosphere.

3.1 Variation of Soil Albedo

The broadband blue-sky albedo (α) overall level of arable lands in the mid-latitudes varies substantially between seasons. It reaches the highest values of 0.8–0.95 in the winter due to deep fresh snow cover, and the lowest ones, 0.05–0.15, in the spring when the snow abruptly melts on dark-colored, wet rough soils before the emergence of crops (Oke 1987; Dobos 2017). The α level of arable lands gradually increases during crop maturation (Dexter 2004). Throughout the growing season, the α level of cereals increases as a function of plant height, leaf area and canopy cover. After maturation, during senescence, their α level increases again. In lower latitudes, especially on dry bare arable lands with light-colored soils, their α level reaches 0.35–0.4 and is higher than that of lands covered with crops. The growing share of crop cover increases the α level of arable lands with dark-colored soils (Rechid et al. 2005). The α level of dark-colored soils can also be increased by the presence of light-colored residues (Horton et al. 1996).

The α of arable lands, as well as other Earth objects depend not only on their intrinsic properties, but also on their illumination conditions, described by the θ_s, the proportion of the diffuse radiance and the cloud cover. In clear-sky conditions, the α of bare arable lands increases with increasing θ_s, mainly due to irregularities in their surfaces. Monteith and Szeicz (1961) already reported in the 1960s that α a increased from 0.16 to 0.19 in the afternoon when θ_s increased from 30° to 70°. Kondratyev (1969) found that in the morning, when θ_s decreased from 80° to 25°, α of dry stony and loamy soils dropped from 0.22 to 0.14 and from 0.34 to 0.21, respectively. Much later, a similar relationship between θ_s and the narrowband and broadband α of bare soils was reported by Pinty et al. (1989), Lewis and Barnsley (1994), Oguntunde et al. (2006). The lowest α values of bare arable lands are recorded at local solar noontime when θ_s reaches its minimum. However, the soils attained their highest α values of about 1 at sunrise and sunset. Diurnal graphs of the soils' α versus θ_s are U-shaped (Roxy et al. 2010). This dependency can be asymmetrical around solar noon due to the formation of dew or changes in atmospheric conditions during the day (Fraser 1975). The larger part of the diffuse radiation component (which also

can be the effect of greater cloud cover), the weaker the effect of the θ_s variation on α of soils.

3.2 Soil Albedo as a Parameter for Modeling Changes in the Climate of the Earth

The α values of many components of the Earth's surface are fundamental input parameters in modeling the energy flow between them and the atmosphere, and thus in global modeling of the Earth's climate (Ben-Gai et al. 1998; Davin et al. 2007). Smoothing rough, deeply plowed soils with, for example, Hs increases their albedo, which lowers the amount of shortwave radiation absorbed by their surface layer. Those surfaces emit less longwave radiation, reducing their temperature, and when areas of them are large, their reflectance can affect the climate of the Earth (Schneider and Dickinson 1974; Desjardins 2009; Farmer and Cook 2013). The appreciation of soil α variation is particularly important in the view of (Sellers et al. 1995), who defined an acceptable α error of the Earth's surfaces for modeling climate change on a global scale at $\pm 2\%$. The use of average diurnal α_d values (α_d) for such modeling seems more useful than the use of instantaneous values (Grant et al. 2000; Cierniewski et al. 2013).

Nowadays, the α of the Earth's surfaces or their components, such as bare soils, are obtained by means of satellite observation. Because satellite radiometers collect shortwave radiance of the surfaces at one or several directions inside their small field of view, in a number of separate narrowband channels, measuring it at the top of the atmosphere (TOP), the approximation of the α of the surfaces by this raw satellite data needs to be corrected (Pinty and Szejwach 1985; Gutman 1988; Tsvetsinskaya et al. 2006). The estimation of the accuracy of broadband α estimation using satellite data has been made using albedometers mounted on towers from a height of several dozen meters (Liang et al. 2002; Cescatti et al. 2012).

Anticipating that the elimination of even one of these corrective procedures can reduce the error of this approximation, Cierniewski and Gdala (2010) and Cierniewski et al. (2013) considered how correction of the bidirectional reflectance of soils only taking into account the specific direction of satellite viewing (i.e., without taking into account the sun position) can affect the achievement of the soil α values with an error lower than $\pm 2\%$. Cierniewski et al. (2013) analyzed how strongly the roughness of soil surfaces (smooth, moderately rough and very rough) and their latitudinal position affects the optimal time (To) for the soil observation by a satellite in sun-synchronous orbit at selected dates with this acceptable error. It was found that the morning To is expected earliest for the very rough soil, and latest for the smooth soil. In the afternoon this trend is reversed. In certain latitude ranges, the difference between To for smooth soils and for moderately rough soils can be just below 40 min, while the difference between To for very rough and moderately rough soils can be about 15 min. The usefulness of an orbit during the analyzed dates was expressed by the

length along which observation of the soils was available with an acceptable error of ±2%. The longest parts of the orbits—larger than 90°—were predicted for the morning in mid-April, while the shortest, reaching only about 20°, were found for the afternoon in the beginning of the astronomical summer. An attempt was also made to compare the usefulness of satellite orbits crossing the equator at local solar time 7:30 and 10:30, such as for the NOAA-15 and the MODIS Cierniewski (2012). The earlier orbit proved to be much more useful for soil observation in the middle of April and at the end of August in the range larger than 90°, and least useful at the beginning of the astronomical summer in the Northern Hemisphere in the range lower than 30°. The earlier orbits turned out to be much less useful for observing bare soils than the later one.

3.3 *Measurements of Diurnal Blue-Sky Albedo Variation of Soils*

When investigating the diurnal α variation of cultivated and uncultivated surfaces developed from the same soil material in the Israeli Negev desert Cierniewski et al. (2013) found that the soil's roughness not only affects its overall α level under clear-sky conditions, but also the steepness of its α from θ_s at the local solar noon to about 75°. The α values of the surfaces that were deeply plowed barely increased in this θ_s range, while the α values of the soils that were the same but with smoothed surfaces gradually increased. Such an effect of soil roughness on their diurnal α variation (Fig. 24) was confirmed on 81 sets of data collected on arable lands in the southern and central districts in Israel and in the Wielkopolska region of Poland (Cierniewski et al. 2015). Each of these sets, which describe the half-diurnal α distributions of soils and that were collected as in the previous case by LP PYRA 06 albedometers from 1.5–2 m, was accompanied by data characterizing the shape of the soil surfaces formed by such farming tools as planters (Fp), plows (Pd) and disk

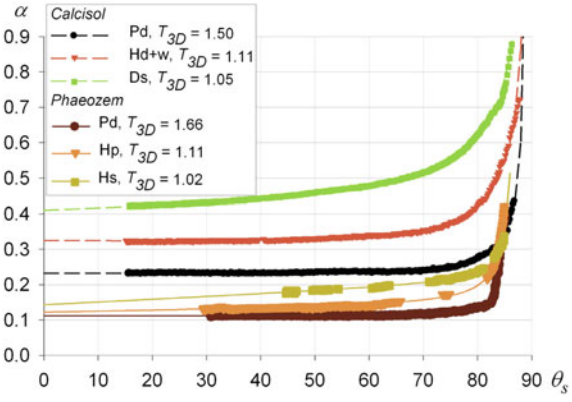

Fig. 24 Variation of the half diurnal broadband blue-sky albedo of a light-colored *Calcisol* formed by a plow (Pd), a disc harrow and modified by sprinkler irrigation (Hd + w) and not cultivated (Ds), as well as a dark-colored *Phaeozem* formed by a plow (Pd), a spike-tooth harrow (Hp), and smoothing harrow (Hs). Shape of the surfaces was quantified by the T_{3D} roughness index

harrows (Hd), pulverizing harrows (Hp) and smoothing harrows (Hs). Modifications of these surfaces due to rainfall or sprinkler irrigation were also taken into account. The shape of the surfaces was measured using stereo-photographs taken by cameras that moved along a leveled construction supported by two tripods, and then as attached to a monopod that, moving around a measured surface, recorded its image from many directions. Additionally, each studied soil's reflectance spectrum in the range 0.35–2.5 μm was measured in the laboratory by a FieldSpec spectroradiometer with a Hi-Brite Muglight receptor, using the procedure that is recommended to collect soil reflectance spectra stored in soil databases in the world (Ben-Dor et al. 2015).

3.4 Equations Predicting Diurnal Blue-Sky Albedo Variation of Soils Taking into Account Their Roughness

The above data, supplemented with values characterizing the contents of soil organic carbon (SOC) and $CaCO_3$ of the studied soils enabled us to determine the following equations (Cierniewski et al. 2015):

$$\alpha_0 = 0.301 - 0.042 \cdot \mathrm{SOC} + 0.007 \cdot \mathrm{CaCO_3} - 0.088 \cdot T_{3\mathrm{D}} \tag{19}$$

$$s_\alpha = 0.0054 \cdot (HSD)^{-1.535}, \tag{20}$$

which enable us to predict the half-diurnal α of a soil surface from the solar noon to $\theta_s = 75°$ depending on its roughness expressed by the *HSD* and T_{3D} indices, where α_0 relates to its theoretical α at $\theta_s = 0°$, and s_α describes the linear slope of the α increase from the solar noon to θ_s of 75°. The correctness of the equations, expressed by the coefficient of determination (R^2) and the root mean square error (RMSE), was estimated at 0.90 and 0.03, respectively.

Carrying out the research project 2014/13/B/ST10/02111, which is supported by the Polish National Science Centre and aims to quantify the annual dynamics of shortwave radiation reflected from arable lands on a global scale taking into account their roughness, the diurnal α distributions of a much larger number of soil units were needed than it was possible to obtain by measuring them directly in the field. Analyzing the correctness of predicting such diurnal α distributions through the aforementioned soil laboratory spectra, it was attempted to determine whether the necessary soil diurnal α distributions could be additionally obtained by their laboratory reflectance spectra stored in the spectral libraries of soils in the world.

The global library of soil reflectance spectra has been being developed since 2008 as a voluntary collaborative project (Viscarra Rossel 2009). By about 2015, this library contained soil reflectance spectra accompanied by chemical and physical attribute data from over 90 countries on seven continents (Viscarra Rossel et al. 2016). This global soil database includes spectra from soil in the World Soil Information collection recorded by the World Agroforestry Centre and also other national,

multinational and continental soil databases. The largest continental database, the European Use and Cover Area frame Statistical Survey (LUCAS), was initiated by a decision of the European Parliament and the Council of the European Union in 2007 (Stevens et al. 2013). The Global Soil Spectral Library and the LUCAS library combined contain over 20,000 such soil spectra of geo-referenced topsoil samples with their chemical and physical attribute data (Viscarra Rossel et al. 2016).

The first set of equations, which predicted the half-diurnal α distributions of a soil surface taking into account its roughness using its soil reflectance spectrum obtained in laboratory conditions, was established on the basis of 108 sets of soil data collected in Poland and Israel (Cierniewski et al. 2017a) in similar way as those mentioned above. The first equation:

$$a_{45} = 0.454 - 0.112T_{3D} + 6952.66d_{474} + 13108.37d_{705} + 12470.20d_{952} - 11597d_{1650} \quad (21)$$

predicts the overall α level of the soil of a given roughness at $\theta_s = 45°$, where d together with its associated number relates to the soil reflectance data transformed to its second derivative for specified wavelength in nm. The second equation:

$$\alpha_{\theta_s} = \alpha_{45}[1 + s_\alpha(\theta_s - 45)], s_\alpha = 0.0008 + 0.00108(T_{3D})^{-20.75} \quad (22)$$

describes its α under $0° < \theta_s > 75°$. The R^2 and RMS values for these equations reached 0.89 and 0.03, respectively. Then, these equations were improved based on number of these data sets being increased to 153 and the improved quality of a newly tested soil population in the northern district of Israel and in three southern regions of France, Mid Pyrenees, Languedoc and Provence (Cierniewski et al. 2018a). These equations, finally determined by examining soils belonging to 22 soil units according to the World Reference Base (WRB) for Soil Resources (IUSS Working Group 2014), were formulated as:

$$a_{45} = 0.33 - 0.1099T_{3D} - 5795.4d_{574} - 510.2d_{1087} + 7787.2d_{1355} + 12161d_{1656} + 6932.8d_{698}, \quad (23)$$

and

$$\alpha_{\theta_s} = \alpha_{45}[1 + s_\alpha(\theta_s - 45)], s_\alpha = 6.26 \cdot 10^{-7} + 0.0043(HSD)^{-1.418} \quad (24)$$

The studied surfaces with the highest roughness formed by Fp and Pd (with average *HSD* and T_{3D} values of 56 mm and 1.4, and 32 mm and 1.6, respectively) were characterized by averaged s_α values of 0.00008 and 0.00005, respectively. On the other hand, average s_α values of the surfaces with the lowest roughness formed by Hs (with average *HSD* of 6 mm and T_{3D} of 1.1) were ten times greater, reaching about 0.0003. The surfaces modified by water drops had a lower roughness than the surfaces formed only by agricultural tools. These modified surfaces in relation to

those originally shaped by Fp and Pd (with average *HSD* and T_{3D} of about 40% and 15% lower, respectively) had averaged s_α values of about 25% and 5% higher, respectively. The surfaces modified by water drops in relation to those originally treated by Hs (described by 40% and 5% lower *HSD* and T_{3D}, respectively) were characterized by s_α value of about 50% higher. The R^2 and RMSE of the last set of the equations were estimated at 0.91 and 0.03, respectively.

For the half-diurnal α variation of soils in the full θ_s range from 0° to 90°, the fitting formulas:

$$\alpha_{\theta_s} = \exp\left(\frac{\mathrm{a} + \mathrm{c}\theta_s}{1 + b\theta_s + d(\theta_s)^2}\right) \tag{25}$$

and

$$\alpha_{\theta_s} = \frac{\mathrm{a} + c(\theta_s)^{0.5}}{1 + b(\theta_s)^{0.5}} \tag{26}$$

were used for data obtained through Eqs. 19 and 20 (Cierniewski et al. 2015, 2018b; Cierniewski and Ceglarek 2018) and Eqs. 21–24 (Cierniewski et al. 2017b, 2018a), respectively, where a, b, c, and d are fitting parameters.

3.5 *Use of Laboratory Data to Predict the Annual Variation of Shortwave Radiation Reflected from Bare Arable Lands Taking into Account Their Roughness*

Equations 19, 20 and 26 were used for estimating the annual dynamics of shortwave radiation reflected from bare air-dried soil surfaces at clear-sky conditions as a consequence of smoothing previously plowed and harrowed arable lands in Poland (Cierniewski et al. 2017b). The input data used for these equations was data describing the contents of SOC and $CaCO_3$ of arable lands in Poland stored in the Land Use/Cover Area Frame Survey (LUCAS) (Tóth et al. 2013) and in the database created for monitoring the properties of arable lands in Poland (Terelak et al. 2008). Equations 21, 22 and 26 were used to quantify the annual variation of shortwave radiation reflected, including in clear-sky conditions from air-dried arable lands in Israel, using reflectance spectra of soils stored in the Israeli Soil Database Library (Cierniewski et al. 2018b). The annual variations of the arable land areas in Poland and Israel were determined with the help of Landsat 8 images recorded for the countries in 2013–2014 and 2013–2015, respectively. The images, recorded by the Operational Land Imager (OLI) instrument of the satellite, included two sample surfaces within two scenes of the satellites located in the eastern and western parts of Poland and the entire territory of Israel within there scenes of the satellite. The

images without snow and with up to 10% of cloud cover were radiometrically calibrated to top-of-atmosphere reflectance (TOA) using metadata, and normalized from different illumination conditions by dividing TOA by the cosine of θ_s. A surface was identified as a bare soil by analyzing the shape of its reflectance (RB) recorded in the following bands (B) of the OLI, i.e., if they fulfilled the following conditions: R2 < R3 < R4 < R5 < R6; R6 > R7; R5/R3 > 1.8; R6 − R5 > 0 in the case of arable lands in Poland, and R3 < R4 < R5 < R6; R6 > R7; R6 − R5 < 1 within the lands in Israel. The above sets of the reflectance conditions were established based on the shape of the spectrum of the dominant soil units located within the contours of arable lands, using digital maps of land use and soils of these countries. The half-diurnal α distributions of the studied soil units generated in the θ_s using the aforementioned sets of equations with the assumption that they have a roughness corresponding to those formed by a Pd, an Hd and an Hs. It was assumed that the roughness, expressed by *HSD* and T_{3D}, was 25 mm and 1.5 for the surfaces shaped by Pd, 10 mm and 1.15 for Hd, and 5 mm and 1.05 for Hs (Cierniewski et al. 2014). The distributions were first matched with θ_s variation for each day of the year from local noon to sunset. Then the distributions were stated in a function of time, replacing θ_s by solar local time. This allowed the average diurnal α value (α_d) to be calculated for each day of the year for averaged air-dried arable lands in the studied countries after using the aforementioned agricultural tools. The examples of average soils located in Poland and Israel show how different their diurnal α distributions can be depending on latitude, date and roughness, and how these variables affect their average diurnal values (Fig. 25). Using an Hs to smoothing soil previously shaped by a Pd in Poland increases its α_d at the beginning of the astronomical winter by about 100% and at the beginning of the astronomical summer by about 65%. For average soils in Israel, located at a lower latitude of about 20°, their α_d increase for the first date is about 45%, and 30% for the second.

The diurnal amounts of shortwave radiation reflected from the lands were estimated by multiplying the total amount of shortwave radiation coming to the lands under clear-sky conditions (formulated by formulas contained in Allen et al. 1998) by the α_d of the lands and their areas. It was found that these areas reached two maxima in spring and late summer in Poland (at the beginning of the second decade of March and the end of the first decade of September) and one maximum in summer until early autumn in Israel (between the end of the second decade of July and the end of the first decade of September). The maxima of shortwave radiation (Rr_d) reflected under the clear-sky from these dried arable lands in Poland formed by Pd and Hs were assessed at about 200 and 320 PJ/day in spring, respectively, and in late summer at 220 and 350 PJ/day (Fig. 26). The Rr_d maximum values for air-dried bare arable lands formed by Pd and Hs in Israel were estimated at about 16 and 23 PJ/day, respectively. These values were approx. 14–15 times lower than the corresponding values for lands in Poland mainly because the total area of these lands in Poland was about 35 times larger, but their α_d and Ri_d values were almost 1.5 times and 1.2 times lower in spring and late summer, respectively, than those in Israel in summer until early autumn.

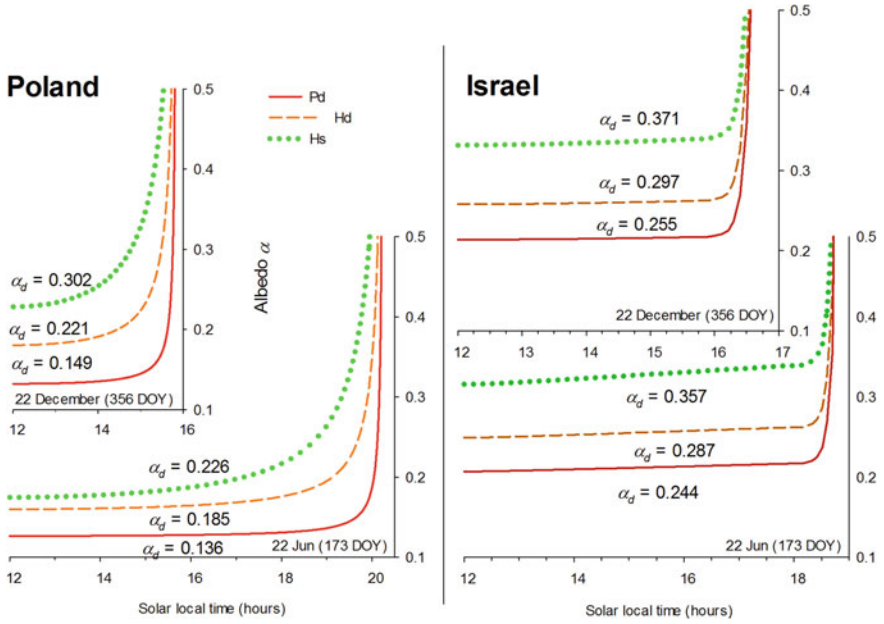

Fig. 25 Half-diurnal albedo distribution of average bare arable lands in Poland and Israel formed by a Pd, an Hd, and an Hs, generated for the shortest (22 December) and the longest (22 June) days, respectively, in relation to the local solar time

In order to estimate the annual dynamics of the shortwave radiation reflected from the bare arable lands on the scale of the European continent Eq. 23, 24 and 25 were used, where thousands of soil reflectance spectra stored in the LUCAS soil database provided input data for these equations to calculate the half-diurnal α variation of the tested lands assuming that they are formed by Pd and Hs and illuminated under clear-sky conditions (Cierniewski et al. 2018c). The use of satellite data from a Spinning Enhanced Visible and Infrared Imager instrument (SEVIRI) (König et al. 2001) made it possible to estimate these dynamics not only under clear-sky conditions, but also in the real changing cloud conditions in the selected year of 2011. The annual variation of the areas of arable lands and periods when they are not covered with crops in such large terrain has been established in a different way than in Poland and Israel. Vectorized and rasterized geostatistical data related to the European Agricultural Region (USDA 1994), divided into three sub-regions limited to member countries of the European Union (EU) together with its associated countries (Switzerland and Norway) were used. The spatial distribution and area of the major crops cultivated there (barley, wheat, maize, potato, rye, sugar beet and rapeseed) was established on the basis of the datasets (Monfreda et al. 2008) in the form of a raster image with a pixel size of 5 × 5 arcmin. The Crop Calendar Dataset (Sacks et al. 2010), containing digitized and georeferenced observation of crop planting and harvesting days (also with the same resolution of 5–5 arcmin) was used to find the date when the crops

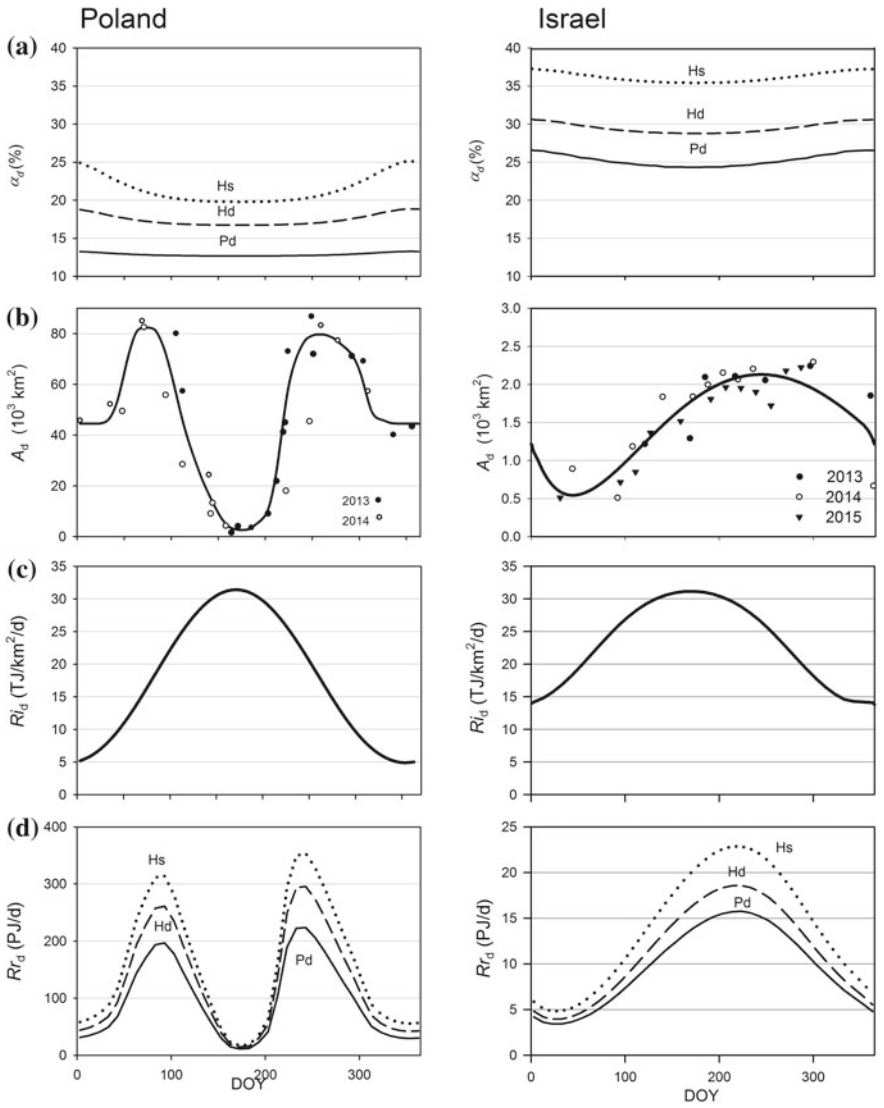

Fig. 26 Annual variation in: **a** average diurnal albedo (α_d) of the average bare arable lands in Poland and Israel, formed by a plow (Pd), a disk harrow (Hd), and a smoothing harrow (Hs); **b** areas of bare arable lands in Poland and Israel extracted from Landsat 8 images; **c** amount of shortwave radiation (Ri_d) reaching the lands in clear-sky conditions; **d** amount of shortwave radiation reflected from all the bare arable lands (Rr_d) within Poland and Israel

were planted. Growing degree days, being a tool for measuring heat accumulation in order to predict the rate of plant development (Miller et al. 2001; Worthington and Hutchinson 2005), was used to determine the period in which crop cover does not exceed 15%, so it could not lose its spectral characteristic as bare soil. To determine the soil units that the delineated arable areas belong to, a digital soil map classified as WRB major reference groups and a land-cover map (GlobCover 2009) were used (Arino et al. 2012). The α_d values of averaged arable lands were generated for each day of the year using half-diurnal α distributions of the air-dried lands in the function of solar local time in the same way as those calculated for these two different size countries—Poland and Israel. Due to the variability of climatic conditions in such a wide area within the EU, α_d values were calculated separately for its western (W), central (C), and southern (S) parts (Fig. 27). Spring peaks of the bare soil areas, about 85,000 and 60,000 km^2, were found within W and C in the middle of first decade of April and in the middle of the first decade of May, respectively. The largest spring peak, reaching 95,000 km^2, was established within S at the turn of the second and the third decade of April. Significantly smaller autumn peaks of the bare soil areas within W, C, and S, reaching 10,000, 20,000, and less than 5000 km^2, respectively, were found at the end of the first decade of October. Within S in summer around the end of the third decade of July an additional area of bare soils was found measuring 10,000 km^2. The average diurnal amount of shortwave radiation reaching the EU's arable lands under changing cloudiness in the selected years of 2011 varied from about 2 TJ/km^2 around the beginning of the astronomical winter to 17, 19, and 21 TJ/km^2 for C, W, and S, respectively, at the beginning of the astronomical summer. It was found finally that the greatest amount of radiation could be reflected from the arable lands of the EU from the beginning of April to the end of May. This instantaneous radiation amount of the soil shaped by a Hs and a Pd was estimated at 250 and 220 PJ/day, respectively, for W, 190 and 150 PJ/day for C, and 330 and 280 PJ/day for S.

In estimating the annual dynamics of short-wave radiation reflected from bare arable lands on a global scale (Cierniewski and Ceglarek 2018), such a procedure for determining the variation of their areas was applied as in the case of the European continent previously discussed, using vectorized and rasterized geostatistical data sets. However, without having the satellite data referring to the real amount of short-wave radiation reaching these lands in this global scale, the estimation was limited only to clear-sky conditions without any clouds. The estimation has been referred to the highest radiation level of the lands, which under conventional tillage (Derpsch et al. 2010) were bare for at least a few days after the day of planting and were air-dried in two extreme roughness states—those shaped by a Pd and those shaped by a Hs. The estimation was carried out on the examples of the thirty-three most extensive agricultural regions on six of the Earth's continents, where thirteen major crops are cultivated (barley, cassava, cotton, groundnut, maize, millet, potato, rapeseed, rye, sorghum, soybean, sugar beet and wheat). This estimate was made using soil units classified as major soil groupings according to the Digital Soil Map of the World (FAO/UNESCO 2007) located within the tested arable lands according to a global land cover map (GlobCover 2009). It was established that the highest peak

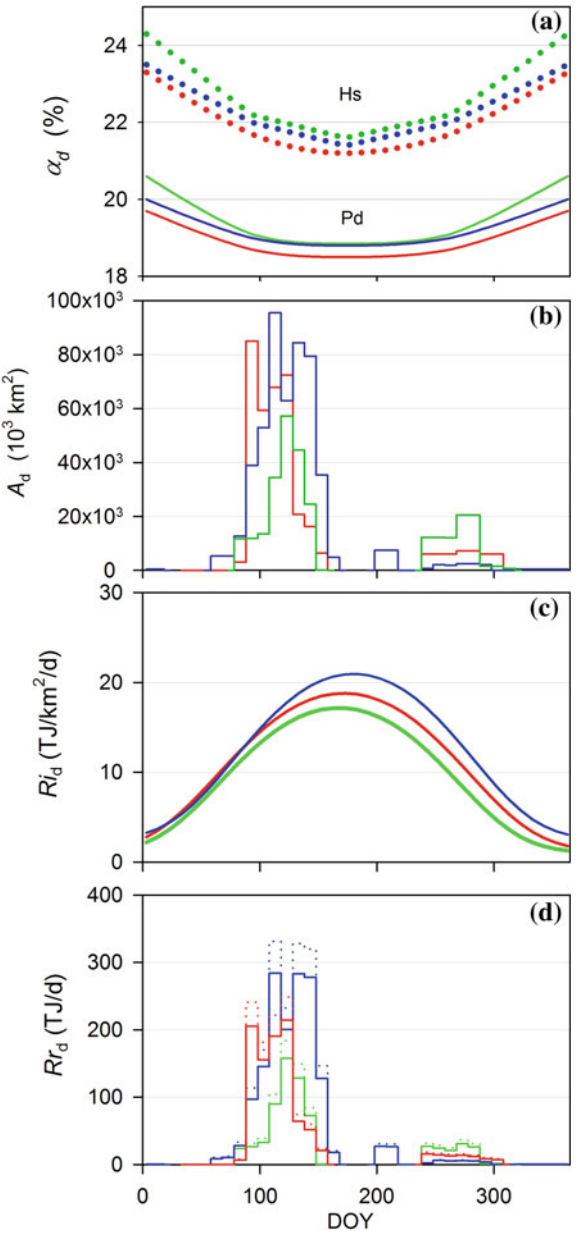

Fig. 27 Annual variation in: **a** average diurnal albedo (α_d) of the average bare arable lands in western (red line), central (green line), and southern (blue line) parts of the European Union (EU), formed by a plow (Pd) and a smoothing harrow (Hs); **b** areas of bare arable lands in these parts of the EUs; **c** real amount of shortwave radiation (Ri_d) reaching the lands in the EU; **d** amount of shortwave radiation reflected from all the bare arable ands (Rr_d), formed by a plow (solid lines) and a smoothing harrow (dashed lines) within these parts of the EU

of shortwave radiation reflected from the lands (Rr_d) formed by a Pd and an Hs in Africa occur in the summer in the middle of the first decade of July, reaching there around 3.5 EJ/day and 4 EJ/day, respectively, when their bare areas reached about 350,000 km^2. In Asia, Europe and North America, the highest Rr_d peaks appear in spring between the beginning and the end of the third decade of May, and in South America at the beginning of the second decade of December. It was found that in this period the total areas of bare arable lands on these continents were about 700,000 km^2, 450,000 km^2, 300,000 km^2, and 500,000 km^2, respectively (Fig. 28). The Rr_d peaks for these extreme roughness states, formed by a Pd and Hs, were evaluated at about 8.5 EJ/day and 10 EJ/day, 5 EJ/day and 8.5 EJ/day, 7 EJ/day and 8.5 EJ/day, and 5.5 EJ/day and 6.3 EJ/day, respectively (Fig. 29). This Rr_d peak appears in Oceania in autumn, in the middle of the first decade of June, reaching

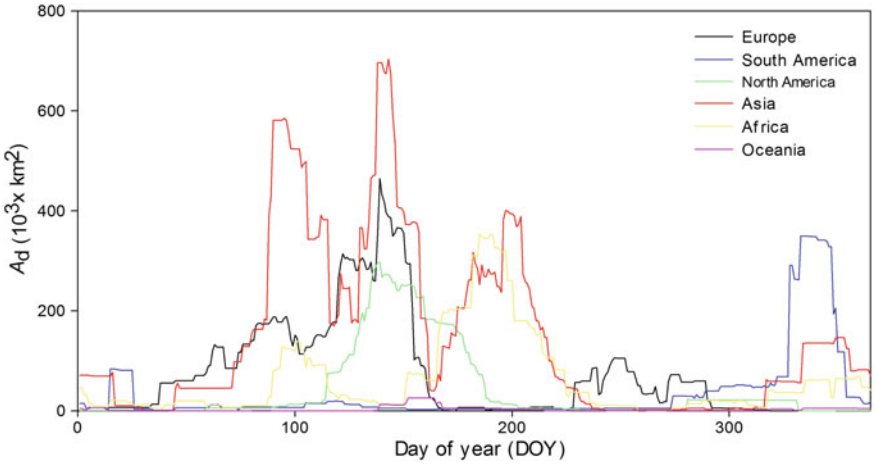

Fig. 28 Annual variation of bare arable land areas (A_d) within six continents of the Earth

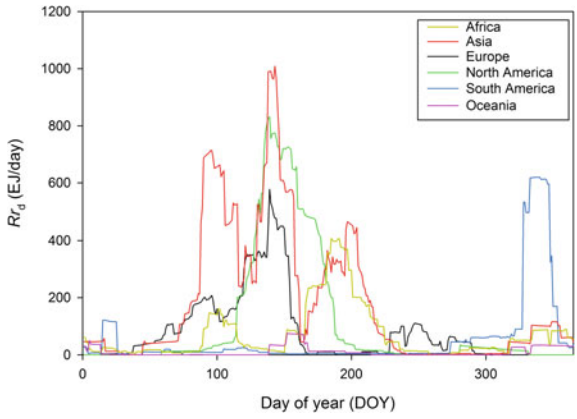

Fig. 29 Annual variation of amount of shortwave radiation reflected from all the bare arable lands formed by a smoothing harrow (Rr_d) within six continents of the Earth

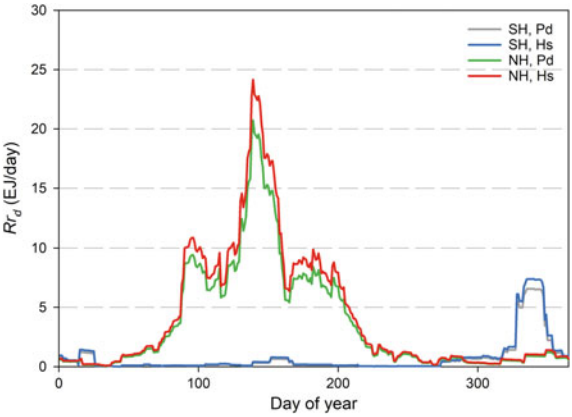

Fig. 30 Annual variation of shortwave radiation reflected from all the bare arable lands (Rr_d), and reflected from bare arable lands formed by a plow (Pd) and a smoothing harrow (Hs) within the Northern Hemisphere (NH) and Southern Hemisphere (SH)

0.15 EJ/day and 0.25 EJ/day. Figure 29 shows the Rr_d values related to these lands formed by a Hs. Aggregating the Rr_d values predicted for the tested agricultural regions located in the Northern Hemisphere, it was found that their highest value occurred at the beginning of the third decade of May reaching 21 EJ/day for soils treated by a Pd, and 24 EJ/day when they are treated by an Hs (Fig. 30).

We suppose that these above values of shortwave radiation reflected and absorbed by bare arable lands in specified periods of the year with their changing areas throughout the year may have a noticeable effect on the Earth's climate on a global scale, depending on the land roughness being the effect of agricultural practices under conventional tillage. Due to the evidently progressive global warming of the climate, forming arable lands under conventional cultivation with the use of agricultural tools that create the lowest possible roughness seems to be one action against this warming. It is assumed that although the annual variation of shortwave radiation reflected from bare arable lands on a global scale is limited to specific conditions, it may facilitate climatologists in more reliable assessment of the impact of these lands on the Earth's climate.

4 Concluding Remarks

This paper discussed the impact of soil properties—those stable in time and those changing dynamically—that have the strongest influence on the bidirectional reflectance (ρ) of soils and their broadband blue-sky albedo (α). However, the impact of soil surface roughness on these physical quantities was discussed here most widely. Models that describe the ρ of soils in changing their illumination and observation condition taking into account this surface feature were used for this purpose.

It is assumed that bare soil surfaces, although appearing in relatively short periods within conventionally cultivated arable lands may, due to their large total areas, can significantly affect the energy transfer between soil, vegetation and the atmosphere,

depending on their spectral reflectance properties (expressed by their α). It is assumed that only one of these properties, which is the roughness of the arable lands, can sufficiently strongly determine this impact. Smoothing rough arable lands that have been previously deeply plowed with, for example, a smoothing harrow increases their α, resulting in a lower amount of shortwave radiation being absorbed by their surface layer. Those surfaces emit less long-wave radiation, leading to reduction in their temperature, which can modify the Earth climate.

This paper presents the sets of equations that make it possible to predict with the satisfactory accuracy the diurnal α using their reflectance spectra obtained under laboratory conditions, which are stored in soil spectral libraries. This variation allows for more precise calculation of the average diurnal α values of soils and, on this basis, also their average α values over longer periods of several days, a month, a season or a year. It is assumed that the application of the procedures for determining the annual variation of shortwave radiation amount reflected from arable lands at such time intervals can improve the accuracy of modeling the Earth's climate change.

Because the surface moisture of arable lands under conventional tillage affects their spectral reflectance as strongly and dynamically as their surface roughness, it would appear important to consider soil moisture as a variables in the newly developed soil reflectance models working in the optical domain.

Estimating the amount of radiation reflected from bare soils on a global scale would be much more realistic if it concerned not only clear-sky conditions, but also the changing cloud conditions on a much larger area than the EU, as has been done thus far using satellite data from the SEVIRI instrument.

In view of the rapid progress of satellite technology, it seems increasingly feasible that a research project can be implemented to confirm the suitability of observation of soil surfaces and other components of the Earth's surface using satellite technology at the optimal time to determine their average diurnal α value.

Acknowledgements This work was supported by the Polish National Science Centre as part of the framework of project no. 2014/13/B/ST10/02111. The author also thanks Jakub Ceglarek for his help in preparation of the figures for this paper.

References

Al-Abbas AH, Swain PH, Baumgardner MF (1972) Relating organic matter and clay content to the multispectral radiance of soils. Soil Sci 114:477–485

Allen RG, Pereira LS, Raes D, Smith M (1998) Crop evapotranspiration: guidelines for computing crop requirements. Irrig Drain Pap No. 56, FAO 300. https://doi.org/10.1016/j.eja.2010.12.001

Andronikov VL (1979) Teoricheskiye osnovy deshifrirovaniya kak metoda izucheniya pochv. Kolos, Moscov (in Rusian)

Arino O, Ramos Perez JJ, Kalogirou V et al (2012) Global land cover map for 2009 (GlobCover 2009). Eur Sp Agency Univ Cathol Louvain

Bachmann CM, Eon R, Ambeau B et al (2017) Modeling and intercomparison of field and laboratory hyperspectral goniometer measurements with G-LiHT imagery of the Algodones Dunes. J Appl Remote Sens 12:1. https://doi.org/10.1117/1.jrs.12.012005

Bauer ME, Vanderbilt VC, Robinson BP, Daugtry CST (1981) Spectral properties of agricultural crops and soils measured space, aerial. In: Field and laboratory sensors. Purdue University

Baumgardner MF, Silva LF, Biehl LL, Stoner ER (1986) Reflectance properties of soils. Adv Agron 38:1–44. https://doi.org/10.1016/s0065-2113(08)60672-0

Ben-Dor E (2002) Quantitative remote sensing of soil properties. 2113:173–243. https://doi.org/10.1016/s0065-2113(02)75005-0

Ben-Dor E, Irons JR, Epema G. (1999) Soil reflectance. In: Rencz E (ed) Remote sensing for earth science: manual of remote sensing. Wiley & Sons Inc, New York, p 111

Ben-Dor E, Goldlshleger N, Benyamini Y et al (2003) The spectral reflectance properties of soil structural crusts in the 1.2 to 2.5 mm spectral region. Soil Sci Soc Am J 67:289–299

Ben-Dor E, Ong C, Lau IC (2015) Reflectance measurements of soils in the laboratory: standards and protocols. Geoderma 245–246:112–124. https://doi.org/10.1016/j.geoderma.2015.01.002

Ben-Gai T, Bitan A, Manes A et al (1998) Spatial and temporal changes in rainfall frequency distribution patterns in Israel. Theor Appl Climatol 61:177–190. https://doi.org/10.1007/s007040050062

Bertuzzi P, Caussignac JM, Stengel P et al (1990) An automated, noncontact laser profile meter for measuring soil roughness in situ. Soil Sci 149:169–178

Białousz S (1978) Zastosowanie Fotointerpretacji do wykonywania map stosunków wodnych gleb. PTG, Pr Kom Nauk 35:1–143 (in Polish)

Białousz S, Girard MG (1978) Wspołczynniki odbicia spectralngo gleb w pasmach pracy satelity landsat. Fotointerpr Geogr 3:111–117 (in Polish)

Biliouris D, Verstraeten WW, Dutré P et al (2007) A Compact Laboratory Spectro-Goniometer (CLabSpeG) to Assess the BRDF of Materials. Presentation, Calibration and Implementation on Fagus sylvatica L. Leaves. Sensors 7:1846–1870. https://doi.org/10.3390/s7091846

Boiffin J (1986) Stages and time-dependency of soil crusting in situ. In: Callebaut F, Gabriels D, De Boodt M (eds) Assessment of soil surface sealing and crusting. University of Ghent, Ghent, Belgium, pp 91–98

Boiffin L, Monnier G (1986) Workshop on erosion assessments for EEC. Methods and models. In: International symposium on assessment of soil surface sealing and crust. Ghent, Belgium, p 4

Bowers SA, Hanks RJ (1965) Reflection of radiant energy from soils. Soil Sci 100:130–138. https://doi.org/10.1097/00010694-196508000-00009

Bowers SA, Smith SJ (1972) Spectrophotometric determination of soil water content. Soil Sci Soc Am J 36:978–980

Brennan B, Bandeen WR (1970) Anisotropic reflectance characteristics of natural earth surfaces. Appl Opt 9:405. https://doi.org/10.1364/ao.9.000405

Cescatti A, Marcolla B, Santhana Vannan SK et al (2012) Intercomparison of MODIS albedo retrievals and in situ measurements across the global FLUXNET network. Remote Sens Environ 121:323–334. https://doi.org/10.1016/j.rse.2012.02.019

Cierniewski J (1985) Relation between soil moisture tension and spectral reflectance of different soils in the visible and near-infrared range. In: Proceedings 3rd international colloquium on spectral signatures of objects in remote sensing. (ESA SP-247), pp 429–432

Cierniewski J (1987) A model for soil surface roughness influence on the spectral response of bare soils in the visible and near-infrared range. Remote Sens Environ 23:97–115. https://doi.org/10.1016/0034-4257(87)90073-3

Cierniewski J (1988) An influence of soil surface moisture and roughness on the spectral response of soil in the visible and near-infrared range, and a mathematical modelling of the relation. Rozpr Nauk Rocz Akad Rol w Pozn 178:1–79 (in Polish)

Cierniewski J (1989) The influence of the viewing geometry of bare rough soil surfaces on their spectral response in the visible and near-infrared range. Remote Sens Environ 27:135–142. https://doi.org/10.1016/0034-4257(89)90013-8

Cierniewski J (1993) Soil moisture tension and soil spectra reflectance on the example of Koscian plain soils. Fotointerpr Geogr 105:107–122
Cierniewski J (1999) Geometrical modeling of soil bi-directional reflectance in the optical domain. Bogucki Sci Publ, Pozn, p 148
Cierniewski J (2001) The bidirectional reflectance model from cultivated soils taking into account soil aggregates and micro-relief. Bogucki Sci Publ, Pozn, p 150 (in Polish)
Cierniewski J (2012) Satellite observation of bare soils for their average diurnal albedo approximation. In: Ist international conference on sensor networks. Rome, Italy, 24–26 February
Cierniewski J, Ceglarek J (2018) Annual dynamics of shortwave radiation of bare arable lands on a global scale incorporating their roughness. Environ Earth Sci 77. https://doi.org/10.1007/s12665-018-7956-7
Cierniewski J, Gdala T (2010) Calculating the optimal time when albedo approximates its daily average: an example using soil surfaces with various roughnesses at different latitudes. Int J Remote Sens 31:2697–2708. https://doi.org/10.1080/01431160903093200
Cierniewski J, Guliński M (2009) Furrow microrelief influence on the directional hiperspectral reflectance of soil at various illumination and observation conditions. IEEE Trans Geosci Remote Sens 48:4143–4148
Cierniewski J, Kuśnierek K (2010) Influence of several soil properties on soil surface reflectance. Quaest Geogr 29:13–25. https://doi.org/10.2478/v10117-010-0002-9
Cierniewski J, Verbrugghe M (1993) A geometrical model of soil bidirectional reflectance in the visible and near-infrared. Fotointerpr Geogr 23:37–51 (in Polish)
Cierniewski J, Verbrugghe M (1994) A geometrical model of soil bidirectional reflectance in the visible and near-infrared range. In: Proceeding 6th international symposium on physical measurements and signatures in remote sensing. Val d'Isére, France, 17–21 January 1994, pp 635–642
Cierniewski J, Verbrugghe M (1997a) Influence of soil surface roughness on soil bidirectional reflectance. Int J Remote Sens 18:1277–1288. https://doi.org/10.1080/0143116972184l2
Cierniewski J, Verbrugghe M (1997b) Inferring soil surface roughness from soil bidirectional reflectance data. Int Agrophys 11:147–157
Cierniewski J, Verbrugghe M, Marlewski A (2002) Effects of farming works on soil surface bidirectional reflectance measurements and modelling. Int J Remote Sens, 23:1075–1094
Cierniewski J, Kijowski A, Mizgajski A (1988) The influence of soil moisture on spectral response of soil cover in the sensitive region of infrared film. In: Proceeding 3rd symposium of the ISSS Working Group on Remote Sensing for Soil Survey. Prace Komisji Naukowych PTG, Jablonna, Poland 1981, pp 45–59
Cierniewski J, Baret F, Verbrugghe M et al (1996) Geometrical modelling of soil bidirectional reflectance incorporating specular effects. Int J Remote Sens 17:3691–3704. https://doi.org/10.1080/01431169608949178
Cierniewski J, Gdala T, Karnieli A (2004) A hemispherical–directional reflectance model as a tool for understanding image distinctions between cultivated and uncultivated bare surfaces. Remote Sens Environ 90:505–523. https://doi.org/10.1016/j.rse.2004.01.004
Cierniewski J, Karnieli A, Herrmann I et al (2010) Soil surface illumination at micro-relief scale and soil BRDF data collected by a hyperspectral camera. Int J Remote Sens 31:2151–2157. https://doi.org/10.1080/01431161003610281
Cierniewski J, Karnieli A, Kuśnierek K et al (2013) Approximating the average daily surface albedo with respect to soil roughness and latitude. Int J Remote Sens 34:3416–3424. https://doi.org/10.1080/01431161.2012.716530
Cierniewski J, Karnieli A, Kaźmierowski C, Ceglarek J (2014) A tool for predicting diurnal soil albedo variation in Poland and Israel. In: EARSeL eProceedings, Special Issue: 34th EARSeL Symposium, pp 36–40
Cierniewski J, Karnieli A, Kazmierowski C et al (2015) Effects of soil surface irregularities on the diurnal variation of soil broadband blue-sky albedo. IEEE J Sel Top Appl Earth Obs Remote Sens 8:493–502. https://doi.org/10.1109/jstars.2014.2330691

Cierniewski J, Ceglarek J, Karnieli A et al (2017a) Predicting the diurnal blue-sky albedo of soils using their laboratory reflectance spectra and roughness indices. J Quant Spectrosc Radiat Transf 200:25–31. https://doi.org/10.1016/j.jqsrt.2017.05.033

Cierniewski J, Królewicz S, Kaźmierowski C (2017b) Annual dynamics of shortwave radiation as consequence of smoothing of previously plowed and harrowed soils in Poland. J Appl Meteorol Climatol 56:735–743. https://doi.org/10.1175/jamc-d-16-0126.1

Cierniewski J, Ceglarek J, Karnieli A et al (2018a) Shortwave radiation affected by agricultural practices. Remote Sens 10. https://doi.org/10.3390/rs10030419

Cierniewski J, Ceglarek J, Kaźmierowski C (2018b) Predicting the Diurnal Blue-Sky albedo variation of soil with given roughness using their hyperspectral reflectance spectra obtained under laboratory conditions. Remote Sens

Cierniewski J, Ceglarek J, Kaźmierowski C, Roujean JL (2018c) Combined use of remote sensing and geostatistical data sets for estimating the dynamics of shortwave radiation of bare arable soils in Europe. Int J Remote Sens 40:1–16. https://doi.org/10.1080/01431161.2018.1474530

Cipra JE, Baumgardner MF, Stoner ER, MacDonald RB (1971) Measuring radiance characteristics of soil with a field spectroradiometer 1. Soil Sci Soc Am J 35:1014. https://doi.org/10.2136/sssaj1971.03615995003500060043x

Clark RN, Swayze GA, Livo KE et al (2003) Imaging spectroscopy: earth and planetary remote sensing with the USGS Tetracorder and expert systems. J Geophys Res 108:1–2. https://doi.org/10.1029/2002je001847

Coburn CA, Peddle DR (2006) A low-cost field and laboratory goniometer system for estimating hyperspectral bidirectional reflectance. Can J Remote Sens 32:244–253. https://doi.org/10.5589/m06-021

Collinet J, Valentin C (1985) Evaluation of factors influencing water erosion in west Africa using rainfall simulation. Challenges in Africa Hydrology and water resources. IAHS Publ 144:451–461

Cooper KD, Smith JA (1985) A monte carlo reflectance model for soil surfaces with three-dimensional structure. IEEE Trans Geosci Remote Sens GE-23:668–673. https://doi.org/10.1109/tgrs.1985.289385

Coulson KL, Reynolds DW (1971) The spectral reflectance of natural surfaces. J Appl Meteorol 10:1285–1295

Croft H, Anderson K, Kuhn NJ (2012) Reflectance anisotropy for measuring soil surface roughness of multiple soil types. CATENA 93:87–96. https://doi.org/10.1016/j.catena.2012.01.007

Croft H, Anderson K, Brazier RE, Kuhn NJ (2013) Modeling fine-scale soil surface structure using geostatistics. Water Resour Res 49:1858–1870. https://doi.org/10.1002/wrcr.20172

Cruse RM, Linden DR, Radke JK et al (1980) A model to predict tillage effects on soil temperature. Soil Sci Soc Am J 44:378–383. https://doi.org/10.2136/sssaj1980.03615995004400020034x

Curran PJ, Foody GM, Kondratyev K Ya, Kozodyrov VV, Fedchenko PP (1990) Remote sensing of soils and vegetation in the USSR. Taylor & Francis, London, New York Philadelphia

Dalal RC, Henry RJ (1986) Simultaneous determination of moisture, organic carbon, and total nitrogen by near infrared reflectance spectrophotometry 1. Soil Sci Soc Am J 50:120. https://doi.org/10.2136/sssaj1986.03615995005000010023x

Davin EL, de Noblet-Ducoudré N, Friedlingstein P (2007) Impact of land cover change on surface climate: Relevance of the radiative forcing concept. Geophys Res Lett 34. https://doi.org/10.1029/2007gl029678

de Jong SM, Addink EA, van Beek LPH, Duijsings D (2011) Physical characterization, spectral response and remotely sensed mapping of mediterranean soil surface crusts. CATENA 86:24–35. https://doi.org/10.1016/j.catena.2011.01.018

Deering DW, Eck TF, Otterman J (1989) Bidirectional reflectances of three soil surfaces and their characterization through model inversion. In: Proceeding of IGARSS '89. IEEE Publications, New York, Vancouver, pp 670–673

Deering DW, Eck TF, Otterman J (1990) Bidirectional reflectances of selected desert surfaces and their three-parameter soil characterization. Agric For Meteorol 52:71–93. https://doi.org/10.1016/0168-1923(90)90101-b

Derpsch R, Friedrich T, Kassam A, Hongwen L (2010) Current status of adoption of no-till farming in the world and some of its main benefits. Int J Agric Biol Eng 3:1–25. https://doi.org/10.3965/j.issn.1934-6344.2010.01.001-025

Desjardins R. (2009) The impact of agriculture on climate change. In: Eagleshham A, Hardy RWFA (eds) Proceeding of the 21st annual of the NABC conference on adapting agriculture to climate change symposium. National Agricultural Biotechnology Council, Saskatoon, SK, Canada, pp 29–39

Desmet A, Evens H, Gombeer R (1988)). Influence of some factors on the reflectance of bare soils. Pedologie 38:227–247

Dexter R (2004) Diunal and seasonal albedo trends of wheat at the Bratt's Lake Observatory, Saskatchewan. MSc Thesis 125

Di Girolamo L (2003) Generalizing the definition of the bi-directional reflectance distribution function. Remote Sens Environ 88:479–482. https://doi.org/10.1016/j.rse.2003.07.004

Dobos E (2017) Albedo. Encyclopedia of soil science, 3rd edn. Taylor & Francis

Epiphanio JCN, Vitorello I (1984) Inter-relationships between view angles (azimuth) and surface moisture and roughness conditions in field-measured radiometer reflectance of an Oxisol. Colloq l'INRA 23:185–192

Eshel G, Levy GJ, Singer MJ (2004) Spectral reflectance properties of crusted soils under solar illumination. Soil Sci Soc Am J 68:1982. https://doi.org/10.2136/sssaj2004.1982

Evans R (1979) Air photos for soil survey in lowland England: factors affecting the photographic images of bare soils and their relevance to assessing soil moisture content and discrimination of soils by remote sensing. Remote Sens Environ 8:39–63. https://doi.org/10.1016/0034-4257(79)90023-3

FAO/UNESCO (2007) Digital soil map of the world. In: Fao-un—l. Water Div. http://www.fao.org/geonetwork/srv/en/metadata.show?id=14116. Accessed 20 June 2017

Farmer TG, Cook J (2013) Climate change science: a modern synthesis. The physical climate, vol 1

Fedchenko PP (1982) Opredeleniye soderzhaniya gumusa v pochvach po ich cvetu. Pochvoved 10:138–141 (in Russian)

Foody GM (1988) The effects of viewing geometry on image classification. Int J Remote Sens 9:1909–1915. https://doi.org/10.1080/01431168808954989

Fraser RS (1975) Interaction mechanisms within the atmosphere (Chap. 5). In: Manual of remote sensing. American Society of Photogrammetry, Falls Church, VA, pp 181–233

Gerbermann AH, Weber DD (1979) Reflectance of varying mixtures of a clay soil and sand. Photogramm Eng Rem Sens 45:1145–1151

Ghishi G, Morgan RPC (1986) Soil erosion in the European Community. Impact in changing Agriculture. In: Proceedings of a seminar on Land degradation due to to hydrological phenomena in hilly areas. Impact of change of land use and management. Cesena, Italy, p 233

Gilley JE, Kottwitz ER (1995) Random Roughness Assessment by the Pin and Chain Method. Appl Eng Agric 12:39–43. https://doi.org/10.13031/2013.25437

Gilliot J-M, Vaudour E, Michelin J (2017) Soil surface roughness measurement: a new fully automatic photogrammetric approach applied to agricultural bare fields

Girard MC, Białousz S (1989) Characteristics of soils in function of their properties. In: Proceeding 3rd symposium of the ISSS Working Group on remote sensing for soil survey. Prace Komisji Naukowych PTG, Jabłonna, Poland, 1981, pp 105:140–147

Goldshleger N, Ben-Dor E, Benyamini Y, Agassi M (2004) Soil reflectance as a tool for assessing physical crust arrangement of four typical soils in Israel. Soil Sci 169:677–687

Gomez C, Lagacherie P, Coulouma G (2008a) Continuum removal versus PLSR method for clay and calcium carbonate content estimation from laboratory and airborne hyperspectral measurements. Geoderma 148:141–148. https://doi.org/10.1016/j.geoderma.2008.09.016

Gomez C, Viscarra Rossel RA, McBratney AB (2008b) Soil organic carbon prediction by hyperspectral remote sensing and field vis-NIR spectroscopy: an Australian case study. Geoderma 146:403–411. https://doi.org/10.1016/j.geoderma.2008.06.011

Graetz R, Gentle M (1982) The relationships between reflectance in the Landsat wavebands and the composition of an Australian semi-arid shrub rangeland. Photogramm Eng Remote Sens 48:1721–1730

Grant IF, Prata AJ, Cechet RP (2000) The impact of the diurnal variation of albedo on the remote sensing of the daily mean albedo of grassland. J Appl Meteorol 39:231–244. https://doi.org/10.1175/1520-0450(2000)039%3c0231:tiotdv%3e2.0.co;2

Gutman G (1988) A simple method for estimating monthly mean albedo of land surfaces from AVHRR data. J Appl Meteorol 27:973–988. https://doi.org/10.1175/15200450(1988)027%3c0973:ASMFEM%3e2.0.CO;2

Hapke B (1981) Bidirectional reflectance spectroscopy. J Geophys Res 86:3039–3054. https://doi.org/10.1016/j.icarus.2008.01.003

Hapke B (1984) Bidirectional reflectance spectroscopy. 3. Correction for macroscopic roughness. Icarus 59:41–59. https://doi.org/10.1016/0019-1035(84)90054-x

Hapke B (1986) Bidirectional reflectance spectroscopy. 4. The extinction coefficient and the opposition effect. Icarus 67:264–280. https://doi.org/10.1016/0019-1035(86)90108-9

Hapke B (1993) Theory of reflectance and emittance spectroscopy. Cambridge University Press, New York

Hapke B (2002) Bidirectional reflectance spectroscopy. 5. The coherent backscatter opposition effect and anisotropic scattering. Icarus 157:523–534. https://doi.org/10.1006/icar.2002.6853

Hapke B (2008) Bidirectional reflectance spectroscopy. 6. Effects of porosity. Icarus 195:918–926. https://doi.org/10.1016/j.icarus.2008.01.003

Harms JD, Bachmann CM, Ambeau BL et al (2017) Fully automated laboratory and field-portable goniometer used for performing accurate and precise multiangular reflectance measurements. J Appl Remote Sens 11:1. https://doi.org/10.1117/1.jrs.11.046014

Henderson TL, Baumgardner MF, Franzmeier DP et al (1992) High dimensional reflectance analysis of soil organic matter. Soil Sci Soc Am J 56:865. https://doi.org/10.2136/sssaj1992.03615995005600030031x

Horton R, Bristow KL, Kluitenberg GJ, Sauer TJ (1996) Crop residue effects on surface radiation and energy balance—review. Theor Appl Climatol 54:27–37. https://doi.org/10.1007/bf00863556

Huang C, White I, Thwaite EG, Bendeli A (1988) A noncontact laser system for measuring soil surface topography. Soil Sci Soc Am J 52:350–355. https://doi.org/10.2136/sssaj1988.03615995005200020009x

Huete AR (1987) Soil and sun angle interactions on partial canopy spectra. Int J Remote Sens 8:1307–1317. https://doi.org/10.1080/01431168708954776

Hunt GR, Salisbury JW (1970) Visible and near infrared spectra of material and rocks. 1. Silicate minerals. Mod Geol 1:283–300

Idso SB, Jackson RD, Reginato RJ et al (1975) The dependence of bare soil albedo on soil water content. J Appl Meteorol Climatol 14:109–113

Irons JR, Campbell GS, Norman JM et al (1992) Prediction and measurement of soil bidirectional reflectance. IEEE Trans Geosci Remote Sens 30:249–260. https://doi.org/10.1109/36.134075

IUSS Working Group WRB (2014) World reference base for soil resources 2014. International soil classification system for naming soils and creating legends for soil maps

Jackson RD, Moran MS, Slater PN, Biggar SF (1987) Field calibration of reference reflectance panels. Remote Sens Environ 22:145–158

Jackson RD, Teillet PM, Slater PN et al (1990) Bidirectional measurements of surface reflectance for view angle corrections of oblique imagery. Remote Sens Environ 32:189–202. https://doi.org/10.1016/0034-4257(90)90017-g

Jacquemoud S, Baret F, Hanocq JF (1992) Modeling spectral and bidirectional soil reflectance. Remote Sens Environ 41:123–132

Jon Ranson K, Biehl LL, Bauer ME (1985) Variation in spectral response of soybeans with respect to illumination, view and canopy geometry. Int J Remote Sens 6:1827–1842. https://doi.org/10.1080/01431168508948331

Karmanova LA (1981) Vliyaniye Razlichnykh form soedineniy zheleza na spektralnuyu sposobnost i cvet. Pochvoved 9:57–64
King C (1979) Contribution á l'utilisation des micro-ondes pour l'étude des sols. INAPG
Kondratyev KY (1969) Radiacjonnyje Charakteristiki Atmosfery i Zemnoy Powerchnosti. Gidrometeorologiczeskoye Izdatelstwo, Leningrad, Russia
Kondratyev KY, Fedchenko PP (1980) Vlijanije obrabotki na spektralnye otrazatelnye svojstva pochvy. Pochvoved 12:47–53 (in Russ)
König M, Tjemkes S, Kerkmann J (2001) atmospheric instability parameters derived from MSG SEVIRI observations. Amer Meteor Soc Preprints 336–338
Kononova MM (1956) Gumus glavneyshikh tipov pochv SSSR, ego priroda i puti obrazovaniya. In: Dokl. Sovetskikh uchenykh, VI Mezhdunarod. Kongressu Pochvevedov: Khemiya pochv. Izdatelstvo AN SSSR, p 209 (in Russian)
Kononova MM (1963) Organicheskiye veshchestvo pochvy, Ego priroda, cvoystva i metody izucheniya. In: Izdatelstvo AN SSSR, p 314 (in Russian)
Kriebel KT (1976) On the variability of the reflected radiation field due to differing distributions of the irradiation. Remote Sens Environ 4:257–264
Krishna Murti GSR, Satyanarayana KVS (1971) Influence of chemical characteristics in the development of soil colour. Geoderma 5:243–248. https://doi.org/10.1016/0016-7061(71)90013-9
Lagacherie P, Baret F, Feret JB et al (2008) Estimation of soil clay and calcium carbonate using laboratory, field and airborne hyperspectral measurements. Remote Sens Environ 112:825–835. https://doi.org/10.1016/j.rse.2007.06.014
Latz KRA, Weismiller GE, Van Scoyoc GE, Baumgardner MF (1984) Characteristic variation in spectral reflectance of selected Eroded Alfisols. Soil Sci Soc Am J 48:1130–1134
Lekner J, Dorf MC (1988) Why some things are darker when wet. Appl Opt 27:1278. https://doi.org/10.1364/ao.27.001278
Lewis P, Barnsley MJ (1994) Influence of the sky radiance distribution on various formulations of the earth surface albedo. In: Proceedings of 6th international symposium physical measurements and signatures in remote sensing. Val d'Is.re, pp 707–716
Liang S, Fang H, Chen M et al (2002) Validating MODIS land surface reflectance and albedo products: methods and preliminary results. Remote Sens Environ 83:149–162. https://doi.org/10.1016/s0034-4257(02)00092-5
Lillesand TM, Kiefer RW, Chipman JW (2004) Remote sensing and image interpretation, 5th edn. New York
Linden DR (1979) A model to predict soil water storage as effected by tillage practices. Ph.D. Dissertation. University of Minnesota
Martonchik JV, Bruegge CJ, Strahler AH (2000) A review of reflectance nomenclature used in remote sensing. Remote Sens Environ 19:9–20
Matthias ADD, Fimbres A, Sano EEE et al (2000) Surface roughness effects on soil albedo. Soil Sci Soc Am J 64:1035–1041. https://doi.org/10.2136/sssaj2000.6431035x
Mikhajlova NA, Orlov DS (1986) Opticheskie Svoystva Pochv i Pochvennych Komponentov. Russ Nauk 118
Milfred CJ, Kiefer RW (2010) Analysis of soil variability with repetitive aerial photography1. Soil Sci Soc Am J 40:553. https://doi.org/10.2136/sssaj1976.03615995004000040028x
Miller P, Lanier W, Brandt S (2001) Using growing degree days to predict plant stages. Mont State Univ Ext Serv 9:MT00103 AG 7/2001
Milton EJ, Webb JP (1987) Ground radiometry and airborne multispectral survey of bare soils. Int J Remote Sens 8:3–14. https://doi.org/10.1080/01431168708948611
Mitchell JK, Jones BAJ (1978) Micro-relief surface depression storage: changes during rainfall events and their application to rainfall-runoff models. Can Water Resour J 14:777–802. https://doi.org/10.4296/cwrj0401121
Monfreda C, Ramankutty N, Foley JA (2008) Farming the planet: 2. Geographic distribution of crop areas, yields, physiological types, and net primary production in the year 2000. Global Biogeochem Cycles 22:1–19. https://doi.org/10.1029/2007gb002947

Monteith JL, Szeicz G (1961) The radiation balance of bare soil and vegetation. Q J R Meteorol Soc 87:159–170. https://doi.org/10.1002/qj.49708737205
Moreno RG, Requejo AS, Alonso AMT, Barrington S, Alvarez MCD (2008) Shadow analysis: a method for measuring soil surface roughness. Geoderma 146:201–208. https://doi.org/10.1016/j.geoderma.2008.05.026
Morgan RPC (1985) Soil degradation and soil erosion in the loamy belt of northern Europe. Soil erosion. In: Ghishi & Morgan. Balkema, pp 165–172
Morra MJ, Hall MH, Freeborn LL (1991) Carbon and nitrogen analysis for soil fractions using near-ifrared reflectance spectroscopy. Soil Sci Soc Am J 55:288–291
Mulders MA (1987) Remote Sensing in Soil Science
Music H, Pelletier R (1986) Response of some Thematic Mapper band rations to variation in soil water content. Photogramm Eng Remote Sens 52:1661–1668
Nicodemus F, Richmond J, Hsia J (1977) Geometrical considerations and nomenclature for reflectance. Sci Technol 60:1–52. https://doi.org/10.1109/lpt.2009.2020494
Norman JM, Welles JM, Walter EA (1985) Contrasts among bidirectional reflectance of leaves, canopies, and soils. IEEE Trans Geosci Remote Sens GE-23:659–667. https://doi.org/10.1109/tgrs.1985.289384
Obukhov AI, Orlov DS (1964) Spektralnaya otrazhatelnaya sposobnost glavneysych tipov pochv i vozmoznost ispolzovaniya diffuznogo otrazhenija pri pochvennych issledovaniyach. Pochvoved 28:83–94
Oguntunde PG, Ajayi AE, van de Giesen N (2006) Tillage and surface moisture effects on bare-soil albedo of a tropical loamy sand. Soil Tillage Res 85:107–114. https://doi.org/10.1016/j.still.2004.12.009
Oke TR (1987) Boundary layer climates. Routledge
Onstad CA (1984) Depressional storage on tilled soil surfaces. Trans ASAE 27:729–732. https://doi.org/10.13031/2013.32861
Orlov DS (1966) Kalichestvennye zakony otrazhenija sveta ot pochvy. Vlijanie razmera chasti na otrazheniye. Nauch Dokl Vys Sk Biol Nauk 4:206–210
Orlov DS (1969) Kalichestvennye zakony otrazhenija sveta ot pochvy. Vlijanie razmera chasti na otrazheniye. Nauch Dokl Vys Sk Biol Nauk 4:26–210
Orlov DS, Sukhanova NI (1983) Vliyanije gumusa na otrazhatelnuyu sposobnost pochv podzony yuzhnoy taygi. Pochvoved 10:43–51
Orlov DS, Bidabayeva RM, Sadovnikov YN (1976) Kalichestvennye zakony otrazheniya sveta ot pochvy. VII.Spektralnye otrazheniye glavnykh pochv Kazakhstana. Nauchnye Dokl Vyss Shkoly Biol Nauk 20:109–113
Otterman J (1981) Reflection from soil with sparse vegetation. Adv Sp Res 1:115–119. https://doi.org/10.1016/0273-1177(81)90387-2
Otterman J (1985) Bidirectional and hemispheric reflectivities of a bright soil plane and a sparse dark canopy. Int J Remote Sens 6:897–902. https://doi.org/10.1080/01431168508948512
Palmer JM (1982) Field standards of reflectance. Photogramm Eng Remote Sensing 48:1623–1625
Peter Heng BC, Chandler JH, Armstrong A (2010) Applying close range digital photogrammetry in soil erosion studies. Photogramm Rec 25:240–265. https://doi.org/10.1111/j.1477-9730.2010.00584.x
Philpot WD (2010) Spectral reflectance of wetted soils. Art Sci Appl Reflectance Spectrosc 1–11. https://doi.org/10.13140/2.1.2306.0169
Piech KR, Walker JE (1974) Interpretation of soils. Photogramm Eng 40:87–94
Pinty B, Szejwach G (1985) A new technique for inferring surface albedo from satellite observations. J Clim Appl Meteorol 24:741–750. https://doi.org/10.1175/1520-0450(1985)024%3c0741:antfis%3e2.0.co;2
Pinty B, Verstraete MM, Dickinson RE (1989) A physical model for predicting bidirectional reflectances over bare soil. Remote Sens Environ 27:273–288. https://doi.org/10.1016/0034-4257(89)90088-6

Potter KN, Horton R, Cruse RM (1987) Soil surface roughness effects on radiation reflectance and soil heat Flux1. Soil Sci Soc Am J 51:855. https://doi.org/10.2136/sssaj1987.03615995005100040003x

Pratt PF (1961) Effect of pH on the cation-exchange capacity of surface soils. Soil Sci Soc Am J 25:96–98. https://doi.org/10.2136/sssaj1961.03615995002500020008x

Rechid D, Jacob D, Hagemann S, Raddatz TJ (2005) Vegetation effect on land surface albedo: method to separate vegetation albedo from the underlying surface using satellite data. Geophys Res Abstr 7:07153

Rieke-Zapp DH, Nearing MA (2005) Digital close range photogrammetry for measurement of soil erosion. Photogramm Rec 20:69–87. https://doi.org/10.1111/j.1477-9730.2005.00305.x

Römkens MJM, Wang JY (1986) Effects of tillage on surface roughness. Trans ASAE 29:429–433

Rosa DJ, Cooper M, Darboux F, Medeiros JC (2012) Soil roughness evolution in different tillage systems under simulated rainfall using a semivariogram-based index. Soil Tillage Res 124:226–232. https://doi.org/10.1016/j.still.2012.06.001

Roxy MS, Sumithranand VB, Renuka G (2010) Variability of soil moisture and its relationship with surface albedo and soil thermal diffusivity at astronomical observatory, Thiruvananthapuram, South Kerala. J Earth Syst Sci 119:507–517. https://doi.org/10.1007/s12040-010-0038-1

Sacks WJ, Deryng D, Foley JA, Ramankutty N (2010) Crop planting dates: an analysis of global patterns. Glob Ecol Biogeogr 19:607–620. https://doi.org/10.1111/j.1466-8238.2010.00551.x

Sandmeier SR (2000) Acquisition of bidirectional reflectance factor data with field goniometers. Remote Sens Environ 73:257–269. https://doi.org/10.1016/s0034-4257(00)00102-4

Schaepman-Strub G, Schaepman ME, Painter TH et al (2006) Reflectance quantities in optical remote sensing-definitions and case studies. Remote Sens Environ 103:27–42. https://doi.org/10.1016/j.rse.2006.03.002

Schneider SH, Dickinson RE (1974) Climate modeling. Rev Geophys 12:447. https://doi.org/10.1029/rg012i003p00447

Schwanghart W, Jarmer T (2011) Linking spatial patterns of soil organic carbon to topography—a case study from south-eastern Spain. Geomorphology 126:252–263. https://doi.org/10.1016/j.geomorph.2010.11.008

Selige T, Böhner J, Schmidhalter U (2006) High resolution topsoil mapping using hyperspectral image and field data in multivariate regression modeling procedures. Geoderma 136:235–244. https://doi.org/10.1016/j.geoderma.2006.03.050

Sellers PJ, Meeson BW et al (1995) Remote sensing of the land surface for studies of global change: models algorithms experiments. Remote Sens Environ 4257:3–26

Shoshany M (1993) Roughness-reflectance relationship of bare desert terrain: an empirical study. Remote Sens Environ 45:15–27. https://doi.org/10.1016/0034-4257(93)90078-c

Stevens A, Nocita M, Tóth G et al (2013) Prediction of Soil Organic Carbon at the European Scale by Visible and Near InfraRed Reflectance Spectroscopy. PLoS One 8. https://doi.org/10.1371/journal.pone.0066409

Stevens A, Udelhoven T, Denis A, Tychon B, Lioy R, Hoffmann L, van Wesemael B (2010) Measuring soil organic carbon in croplands at regional scale using airborne imaging spectroscopy. Geoderma 158:32–45

Stoner ER, Baumgardner MF, Biehl LL, Robinson BF (1980) Atlas of soil reflectance properties. Agricultural Experiment Statio, Purdue University, West Lafayette, Indiana (Res Bull 962)

Swain PH (1978) Remote sensing: the quantitative approach. Mc-Graw Hill, New York

Taconet O, Ciarletti V (2007) Estimating soil roughness indices on a ridge-and-furrow surface using stereo photogrammetry. Soil Tillage Res 93:64–76. https://doi.org/10.1016/j.still.2006.03.018

Terelak H, Stuczynski T, Motowicka-Terelak T et al (2008) Monitoring of chemistry of arable soils in Poland in 2005–2007. In: Inspection of Environmental Protection. Warsaw, Rep, p 135 (in Polish)

Thomsen LM, Baartman JEM, Barneveld RJ, Starkloff T, Stolte J (2015) Soil surface roughness: comparing old and new measuring methods and application in a soil erosion model. Soil 1:399–410. https://doi.org/10.5194/soil-1-399-2015

Tolchelnikov I (1974) Opticheskiye svoystva landshafta. Leningrad
Tóth G, Jones A, Montanarella L (2013) The LUCAS topsoil database and derived information on the regional variability of cropland topsoil properties in the European Union. Environ Monit Assess 185:7409–7425. https://doi.org/10.1007/s10661-013-3109-3
Tsvetsinskaya EA, Schaaf CB, Gao F et al (2006) Spatial and temporal variability in moderate resolution imaging spectroradiometer-derived surface albedo over global arid regions. J Geophys Res Atmos 111:1–10. https://doi.org/10.1029/2005jd006772
Twomey SA, Bohren CF, Mergenthaler JL (1986) Reflectance and albedo differences between wet and dry surfaces. Appl Opt 25:431. https://doi.org/10.1364/ao.25.000431
Ulaby FT, Moore RK, Fung AK (1982) Microwave remote sensing active and passive. Addison-Wesley, Reading, Massachusetts
UN Sustainable Development Knowledge Platform (2015) Open working group proposal for sustainable development goals
USDA (1994) Major world crop areas and climatic profiles. In: agricultural handbook. World Agricultural Outlook Board
Van der Heide G, Koolen AJ (1980) Soil surface albedo and multispectral reflectance of short-wave radiation as a function of degree of slacking. NethJ Agric Sci 28:252–258
Vermang J, Norton LD, Baetens JM et al (2013) Quantification of soil surface roughness evolution under simulated rainfall. Am Soc Agric Eng 56:505–514. https://doi.org/10.13031/2013.42670
Vinogradov BV (1976) Issledovaniye pochvennovo pokrova. In: Kosmicheskiye metody izucheniya sredy. (in Russian). Mysl, Moscov
Vinogradov BV (1981) Distancyonnaya indikaciya soderzhaniya gumusa v pochvach. Pochvoved 11:114–123
Vinogradov BV (1983) Kolichesvennoya vyrazheniye funkci distacyonnoy indikacii vlazhnostii pochv. Dokl Akad Nauk SSR 272:247–250
Viscarra Rossel R (2009) The Soil Spectroscopy Group and the development of a global soil spectral library. NIR News 20:14. https://doi.org/10.1255/nirn.1131
Viscarra Rossel RA, Behrens T, Ben-Dor E et al (2016) A global spectral library to characterize the world's soil. Earth Sci Rev 155:198–230. https://doi.org/10.1016/j.earscirev.2016.01.012
Walthall CL, Norman JM, Welles JM et al (1985) Simple equation to approximate the bidirectional reflectance from vegetative canopies and bare soil surfaces. Appl Opt 24:383. https://doi.org/10.1364/ao.24.000383
Wang Z, Coburn CA, Ren X, Teillet PM (2012) Effect of soil surface roughness and scene components on soil surface bidirectional reflectance factor. Can J Soil Sci 92:297–313. https://doi.org/10.4141/cjss2011-069
White JL (1971) Interpretation of infrared spectra of soil minerals. Soil Sci 112:22–29
Worthington C, Hutchinson C (2005) Accumulated growing degree days as a model to determine key developmental stages and evaluate yield and quality of potat. Proc Fla State Hort Soc 1:98–101
Zobeck TM, Onstad CA (1987) Tillage and rainfall effects on random roughness: a review. Soil Till Res 9:1–20